Aziridination of Alkenes and Amidation of Alkanes by Bis(tosylimido)ruthenium(VI) Porphyrins. A Mechanistic Study

Sze-Man Au, Jie-Sheng Huang, Wing-Yiu Yu, Wai-Hong Fung, and Chi-Ming Che*

Contribution from the Department of Chemistry, The University of Hong Kong, Pokfulam Road, Hong Kong, China

Received April 26, 1999

Abstract: Bis(tosylimido)ruthenium(VI) porphyrins, [Ru^{VI}(Por)$(NTs)_2$] (Por = TPP, TTP, 4-Cl-TPP, 4-MeO-TPP, OEP), were prepared in 60−74% yields by treatment of [Ru^{II}(Por)(CO)(MeOH)] with (*N*-(*p*-tolylsulfonyl)-imino)phenyliodinane (PhI=NTs) in dichloromethane. In dichloromethane containing pyrazole, they reacted with alkenes or alkanes to give tosylamidoruthenium(IV) porphyrins, [Ru^{IV}(Por)(NHTs)(pz)], in about 75% yields. The reactions of [Ru^{VI}(TPP)$(NTs)_2$] and [Ru^{VI}(OEP)$(NTs)_2$] with styrene, para-substituted styrenes, norbornene, cyclooctene, and β-methylstyrene afforded the corresponding *N*-tosylaziridines in 66−85% yields. The aziridination of *cis*-stilbene and *cis*-β-methylstyrene by [Ru^{VI}(Por)$(NTs)_2$] is nonstereospecific with a partial loss of the alkene stereochemistry. Kinetic studies on the reactions between [Ru^{VI}(TPP)$(NTs)_2$] and 16 alkenes (cyclooctene, norbornene, 2,3-dimethyl-2-butene, styrene, para-substituted styrenes, α- and β-methylstyrene, and α- and β-deuteriostyrene) gave the second-order rate constants (k_2) ranging from $(1.60 \pm 0.06) \times 10^{-3}$ to $(90 \pm 4) \times 10^{-3}$ dm^3 mol^{-1} s^{-1} at 298 K. The slope of the linear plot of log k_2 vs $E_{1/2}$ for eight representative alkenes was found to be -1.7 V^{-1}. In the case of para-substituted styrenes, linear correlation between log k_R (k_R = relative rate) and σ^+ gives a ρ^+ value as small as -1.1. However, the effect of para substituents on k_R can be best accounted for by considering both the polar and spin delocalization effect. Measurements on the secondary deuterium isotope effect revealed that only the β-carbon atom of styrene experienced a significant change in its hybridization in reaching the transition state. All these are consistent with rate-determining formation of a carboradical intermediate. The reactions of [Ru^{VI}(TPP)$(NTs)_2$] and [Ru^{VI}-(OEP)$(NTs)_2$] with adamantane, cyclohexene, ethylbenzene, and cumene resulted in tosylamidation of these hydrocarbons and afforded the corresponding amides in 52−88% yields. For cyclohexane and toluene, the tosylamidation products were formed in poor yields (ca. 10%). Kinetic studies on the reactions between [Ru^{VI}-(TPP)$(NTs)_2$] and nine hydrocarbons (cumene, ethylbenzene, cyclohexene, and para-substituted ethylbenzenes) gave the second-order rate constants (k_2) in the range of $(0.330 \pm 0.008) \times 10^{-3}$ to $(16.5 \pm 0.3) \times 10^{-3}$ dm^3 mol^{-1} s^{-1}. These reactions exhibit a large primary deuterium isotope effect, with a k_H/k_D ratio of 11 for the tosylamidation of ethylbenzene. In the case of para-substituted ethylbenzenes, both electron-donating and -withdrawing substituents moderately promote the reaction. There is an excellent linear correlation between log k_R and a related carboradical parameter. On the basis of these observations, a mechanism involving the rate-limiting formation of a carboradical intermediate is postulated.

The development of metal-mediated nitrogen atom transfer reactions such as aziridination of alkenes,[1−10] amination of alkanes,[11] and allylic amination of alkenes[12−16] has received considerable attention in recent years. The best explored systems to date are those employing (*N*-(*p*-tolylsulfonyl)imino)phenyliodinane (PhI=NTs) as the nitrogen source. Although in most cases it is proposed that metal imido species (M=NTs) are crucial intermediates in these reactions, their mechanisms are still poorly understood and remain an open issue. In contrast, there are extensive mechanistic studies in the literature on metal-mediated oxygen atom transfer reactions such as alkene epoxidation.[17]

By analogy with a mechanism postulated for epoxidation by PhI=O, Mansuy and co-workers proposed that the aziridination

(1) Groves, J. T.; Takahashi, T. *J. Am. Chem. Soc.* **1983**, *105*, 2073.
(2) (a) Mansuy, D.; Mahy, J.-P.; Dureault, A.; Bedi, G.; Battioni, P. *J. Chem. Soc., Chem. Commun.* **1984**, 1161. (b) Mahy, J.-P.; Bedi, G.; Battioni, P.; Mansuy, D. *J. Chem. Soc., Perkin Trans. 2* **1988**, 1517.
(3) (a) Evans, D. A.; Faul, M. M.; Bilodeau, M. T. *J. Org. Chem.* **1991**, *56*, 6744. (b) Evans, D. A.; Woerpel, K. A.; Hinman, M. M.; Faul, M. M. *J. Am. Chem. Soc.* **1991**, *113*, 726. (c) Evans, D. A.; Faul, M. M.; Bilodeau, M. T.; Anderson, B. A.; Barnes, D. M. *J. Am. Chem. Soc.* **1993**, *115*, 5328. (d) Evans, D. A.; Faul, M. M.; Bilodeau, M. T. *J. Am. Chem. Soc.* **1994**, *116*, 2742.
(4) (a) Li, Z.; Conser, K. R.; Jacobsen, E. N. *J. Am. Chem. Soc.* **1993**, *115*, 5326. (b) Li, Z.; Quan, R. W.; Jacobsen, E. N. *J. Am. Chem. Soc.* **1995**, *117*, 5889.
(5) O'Connor, K. J.; Wey, S.-J.; Burrows, C. J. *Tetrahedron Lett.* **1992**, *33*, 1001.
(6) Ando, T.; Minakata, S.; Ryu, I.; Komatsu, M. *Tetrahedron Lett.* **1998**, *39*, 309.
(7) Lai, T.-S.; Kwong, H.-L.; Che, C.-M.; Peng, S.-M. *Chem. Commun.* **1997**, 2373.
(8) Noda, K.; Hosoya, N.; Irie, R.; Ito, Y.; Katsuki, T. *Synlett* **1993**, 469.
(9) Müller, P.; Baud, C.; Jacquier, Y. *Tetrahedron* **1996**, *52*, 1543.
(10) Au, S.-M.; Fung, W.-H.; Cheng, M.-C.; Che, C.-M.; Peng, S.-M. *Chem. Commun.* **1997**, 1655.
(11) Breslow, R.; Gellman, S. H. *J. Chem. Soc., Chem. Commun.* **1982**, 1400.
(12) (a) Breslow, R.; Kluttz, R. Q.; Khanna, P. L. *Tetrahedron Lett.* **1979**, 3273. (b) Breslow, R.; Gellman, S. H. *J. Am. Chem. Soc.* **1983**, *105*, 6728.
(13) Mahy, J. P.; Bedi, G.; Battioni, P.; Mansuy, D. *Tetrahedron Lett.* **1988**, *29*, 1927.
(14) Albone, D. P.; Aujla, P. S.; Taylor, P. C. *J. Org. Chem.* **1998**, *63*, 9569.
(15) Au, S.-M.; Zhang, S.-B.; Fung, W.-H.; Yu, W.-Y.; Che, C.-M.; Cheung, K.-K. *Chem. Commun.* **1998**, 2677.
(16) Nägeli, I.; Baud, C.; Bernardinelli, G.; Jacquier, Y.; Moran, M.; Müller, P. *Helv. Chim. Acta* **1997**, *80*, 1087.

10.1021/ja9913481 CCC: $18.00
Published on Web 09/18/1999

of alkenes by PhI═NTs catalyzed by iron porphyrins involves addition of an Fe^{V}═NTs (or Fe^{IV}—NTs) species to the alkene double bond, to form a carboradical intermediate, which yields *N*-tosylaziridines via direct oxidative transfer of the NTs ligand to the intermediate carbon-centered radical or via a four-membered Fe−C−C−N metallocycle.[2b] However, since the metal imido (Fe^{V}═NTs) species could not be isolated, it is hard to assess this mechanism by conventional kinetic methods.

The same problem is also encountered for the aziridination of alkenes by PhI═NTs catalyzed by copper complexes,[3,4] the most efficient catalysts for the aziridination reactions which in some cases also have high enantioselectivity.[3c,4a] It appears that a concerted mechanism is operative, as proposed by Evans and co-workers on the basis of product analysis and solvent effects.[3d] Although the work by Jacobsen and co-workers strongly argues for the intermediacy of a discrete Cu═NTs intermediate in such systems,[4b] in no cases are such intermediates observed and characterized.

While the putative metal imido intermediates in all the known aziridination or amination reactions described above have never been isolated, there are a plethora of metal imido complexes which have been obtained in pure form.[18] However, none of these complexes are found to undergo aziridination reactions with an alkene. To better understand the mechanism of alkene aziridination involving metal imido intermediates, the quest for a metal imido complex that is stable for isolation and yet sufficiently reactive toward aziridination of alkenes is of particular importance.

Recently, we preliminarily reported that treatment of carbonylruthenium(II) porphyrins, [Ru^{II}(Por)(CO)(MeOH)], with PhI═NTs readily affords bis(tosylimido)ruthenium(VI) porphyrins, [Ru^{VI}(Por)$(NTs)_2$], and, strikingly, this type of high-valent ruthenium imido complexes is reactive toward alkenes to give aziridines in good yields.[10] Herein we present a mechanistic study on such reactions by employing conventional kinetic methods. By analogy with the mechanisms proposed for the alkene epoxidations by high-valent metal oxo species,[17] a total of five different pathways involving the intermediates **I** to **V** shown in Scheme 1 should be considered in the case of alkene aziridination. The ultimate goal of this work is to ascertain the most probable pathway on the basis of kinetic results. In addition, we have also found that the tosylimidoruthenium(VI) porphyrins are reactive toward alkanes, leading to insertion of the imido group into the C−H bonds. Mechanistic studies on such amidation processes are also described. After completion of this work, we were informed of the synthesis of [Ru^{VI}(TMP)$(NTs)_2$] complex (TMP = *meso*-tetrakis(2,4,6-trimethylphenyl)-porphyrinato dianion) by Groves and co-workers.[19]

Scheme 1

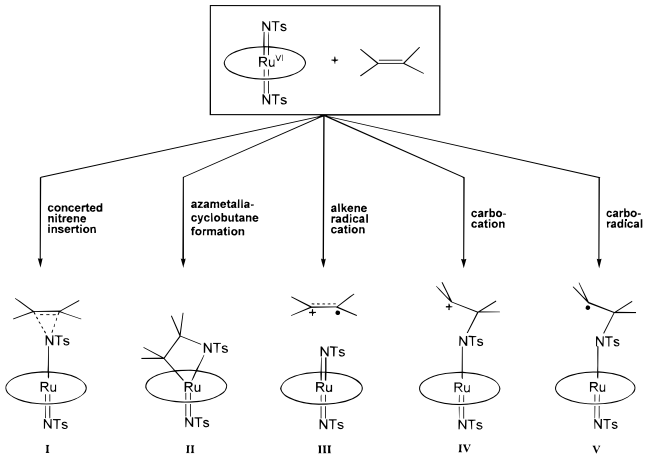

Experimental Section

Materials. Dichloromethane (AR, Ajax) was sequentially washed with concentrated sulfuric acid, deionized water, saturated sodium bicarbonate, and again deionized water and then refluxed over calcium chloride followed by distillation over calcium hydride. Methanol (GR, Merck) and *n*-pentane (AR) were used as received. The following reagents purchased from commercial vendors were further purified before use: norbornene (purified by sublimation); *trans*-stilbene and adamantane (both recrystallized from ethanol); cyclohexene, cyclohexane, *cis*-cyclooctene, and styrene (all distilled from calcium hydride); *cis*-stilbene, 4-methoxystyrene, 4-methylstyrene, 4-chlorostyrene, 4-fluorostyrene, 4-cyanostyrene, 4-acetoxystyrene, 4-trifluoromethylstyrene, 2,3-dimethyl-2-butene, ethylbenzene, cumene, α-methylstyrene, and *trans*-*β*-methylstyrene (all purified by passing through a column of activated alumina). The purity of the alkenes was checked by GC or ^{1}H NMR analysis. *cis*-*β*-Methylstyrene,[20] *cis*-*β*-deuteriostyrene,[20] *β*-d_2-styrene,[21a,b] and α-deuteriostyrene[21a,c] were prepared according to the literature procedures. Cyclohexene-d_{10} and ethylbenzene-d_{10} (both purchased from Aldrich) and all the other commercially available reagents or chemicals were used as received. The carbonylruthenium-(II) porphyrins, [Ru^{II}(Por)(CO)(MeOH)] (**1**) (Por = TPP, **1a**; TTP, **1b**; 4-Cl-TPP, **1c**; 4-MeO-TPP, **1d**; OEP, **1e**),[22] were prepared by the standard method.[23]

General Procedure for the Preparation of [Ru^{VI}(Por)$(NTs)_2$] (2) (Por = TPP, 2a; TTP, 2b; 4-Cl-TPP, 2c; 4-MeO-TPP, 2d; OEP, 2e). A mixture of [Ru^{II}(Por)(MeOH)(CO)] **(1)** (0.05 mmol) and PhI═NTs (0.2 mmol) in dichloromethane (10 mL) was stirred for 5 min at room temperature under a nitrogen atmosphere. Removal of the solvent in vacuo followed by washing the residue with methanol gave a reddish-violet solid. The solid was redissolved in dichloromethane (2 mL) and chromatographed on a short column of neutral alumina with the same solvent as the eluant. The first band was collected and the solvent was removed in vacuo, affording complexes **2a**−**e** in 60−74% yields.

[Ru^{VI}(TPP)$(NTs)_2$] (2a): Anal. Calcd for $C_{58}H_{42}N_6O_4RuS_2$: C, 66.21; H, 4.02; N, 7.99. Found: C, 66.11; H, 4.05; N, 8.02. UV/vis (1.43×10^{-6} M, CH_2Cl_2): λ_{max}/nm (log ϵ) 421 (5.14), 536 (4.18), 568 (3.77). IR (Nujol, cm^{-1}): "oxidation state marker" band 1016. ^{1}H NMR (300 MHz, CD_2Cl_2): H_β 8.82 (8H, s), H_o(eq) 8.18 (8H, m), H_m(eq), H_p(eq) 7.79 (12H, m); H_m(ax) 6.45 (4H, d, J = 8.1 Hz), H_o(ax) 4.87 (4H, d, J = 8.3 Hz), CH_3(ax) 2.17 (6H, s). FAB mass spectrum: m/z 1051 $[M]^+$, 882 $[M - NTs]^+$, 727 $[M - NTs - Ts]^+$, 713 $[M - NTs - NTs]^+$.

(17) (a) Samsel, E. G.; Srinivasan, K.; Kochi, J. K. *J. Am. Chem. Soc.* **1985**, *107*, 7606. (b) Groves, J. T.; Watanabe, Y. *J. Am. Chem. Soc.* **1986**, *108*, 507. (c) Castellino, A. J.; Bruice, T. C. *J. Am. Chem. Soc.* **1988**, *110*, 158. (d) Garrison, J. M.; Bruice, T. C. *J. Am. Chem. Soc.* **1989**, *111*, 191. (e) Garrison, J. M.; Ostovic, D.; Bruice, T. C. *J. Am. Chem. Soc.* **1989**, *111*, 4960. (f) Ostovic, D.; Bruice, T. C. *J. Am. Chem. Soc.* **1989**, *111*, 6511. (g) Ostovic, D.; Bruice, T, C. *Acc. Chem. Res.* **1992**, *25*, 314. (h) Arasasingham, R. D.; He, G. X.; Bruice, T. C. *J. Am. Chem. Soc.* **1993**, *115*, 7985. (i) Groves, J. T.; Gross, Z.; Stern, M. K. *Inorg. Chem.* **1994**, *33*, 5065. (j) Finney, N. S.; Pospisil, P. J.; Chang, S.; Palucki, M.; Konsler, R. G.; Hansen, K. B.; Jacobsen, E. N. *Angew. Chem., Int. Ed. Engl.* **1997**, *36*, 1720. (k) Linde, C.; Arnold, M.; Norrby, P.; Åkermark, B. *Angew. Chem., Int. Ed. Engl.* **1997**, *36*, 1723. (l) Linker, T. *Angew. Chem., Int. Ed. Engl.* **1997**, *36*, 2060. (m) Palucki, M.; Finney, N. S.; Pospisil, P. J.; Güler, M. L.; Ishida, T.; Jacobsen, E. N. *J. Am. Chem. Soc.* **1998**, *120*, 948.

(18) Wigley, D. E. *Prog. Inorg. Chem.* **1994**, *42*, 239.

(19) Groves, J. T. Personal communication.

(20) Lindler, H.; Dubuis, R. *Org. Synth.* **1973**, *5*, 880.

(21) (a) Overberger, G. H.; Saunders, J. H. *Org. Synth.* **1955**, *3*, 204. (b) Hosokawa, T.; Ohta, T.; Kanagama, S.; Murahashi, S.-I. *J. Org. Chem.* **1987**, *52*, 1758. (c) Wesener, J. R.; Maskau, D.; Günther, H. *J. Am. Chem. Soc.* **1985**, *107*, 7307.

(22) Abbreviations: TPP = *meso*-tetraphenylporphyrinato dianion; TTP = *meso*-tetrakis(*p*-tolyl)porphyrinato dianion; 4-Cl-TPP = *meso*-tetrakis(*p*-chlorophenyl)porphyrinato dianion; 4-MeO-TPP = *meso*-tetrakis(*p*-methoxyphenyl)porphyrinato dianion; OEP = octaethylporphyrinato dianion.

(23) Rillema, D. P.; Nagle, J. K.; Barringer, L. F., Jr.; Meyer, T. J. *J. Am. Chem. Soc.* **1981**, *103*, 56.

[Ru^{VI}(TTP)(NTs)$_2$] (2b): Anal. Calcd for $C_{62}H_{50}N_6O_4RuS_2$: C, 67.19; H, 4.55; N, 7.58. Found: C, 67.38; H, 4.61; N, 7.42. UV/vis (1.45×10^{-5} M, CH_2Cl_2): λ_{max}/nm (log ϵ) 423 (5.21), 538 (4.29), 571 (3.88). IR (Nujol, cm^{-1}): "oxidation state marker" band 1016. ^{1}H NMR (300 MHz, CD_2Cl_2): H_β 8.86 (8H,s), H_o(eq) 8.03 (8H, d, J = 8.10 Hz), H_m(eq) 7.58 (8H, d, J = 8.09 Hz), CH_3(eq) 2.73 (12H, s); H_m(ax) 6.48 (4H, d, J = 8.01 Hz), H_o(ax) 4.84 (4H, d, J = 8.25 Hz), CH_3(ax) 2.18 (6H, s). FAB mass spectrum: m/z 1107 [M]$^+$, 938 [M − NTs]$^+$, 783 [M − NTs − Ts]$^+$, 769 [M − NTs − NTs]$^+$.

[Ru^{VI}(4-Cl-TPP)(NTs)$_2$] (2c): Anal. Calcd for $C_{58}H_{38}N_6Cl_4O_4RuS_2$: C, 58.54; H, 3.22; N, 7.06. Found: C, 58.60; H, 3.17; N, 7.11. UV/vis (1.40×10^{-5} M, CH_2Cl_2): λ_{max}/nm (log ϵ) 422 (5.09), 536 (4.20), 569 (3.77). IR (Nujol, cm^{-1}): "oxidation state marker" band 1016. ^{1}H NMR (300 MHz, CD_2Cl_2): H_β(eq) 8.81 (8H, s), H_o(eq) 8.02 (8H, d, J = 8.3 Hz), H_m(eq) 7.73 (8H, d, J = 8.3 Hz); H_m(ax) 6.40 (4H, d, J = 8.2 Hz); H_o(ax) 4.73 (4H, d, J = 8.31 Hz), CH_3(ax) 2.1 (6H, s). FAB mass spectrum: m/z 1189 [M]$^+$, 1020 [M − NTs]$^+$, 865 [M − NTs − Ts]$^+$, 851 [M − NTs − NTs]$^+$.

[Ru^{VI}(4-MeO-TPP)(NTs)$_2$] (2d): Anal. Calcd for $C_{62}H_{50}N_6O_8RuS_2$: C, 63.52; H, 4.30; N, 7.17. Found: C, 63.61; H, 4.40; N, 7.15. UV/vis (1.47×10^{-5} M, CH_2Cl_2): λ_{max}/nm (log ϵ) 426 (5.10), 540 (4.19), 575 (3.91). IR (Nujol, cm^{-1}): "oxidation state marker" band 1019. ^{1}H NMR (300 MHz, CD_2Cl_2): H_β 8.88 (8H, s), H_o(eq) 8.07 (8H, d, J = 8.46 Hz), H_m(eq), 7.34 (8H, d, J = 8.49 Hz), MeO(eq) 4.11 (12H, s); H_m(ax) 6.49 (4H, d, J = 8.13 Hz), H_o(ax) 4.84 (4H, d, J = 8.19 Hz), CH_3(ax) 2.18 (6H, s). FAB mass spectrum: m/z 1171 [M]$^+$, 1002 [M − NTs]$^+$, 847 [M − NTs − Ts]$^+$, 833 [M − NTs − NTs]$^+$.

[Ru^{VI}(OEP)(NTs)$_2$] (2e): Anal. Calcd for $C_{50}H_{58}N_6O_4RuS_2$: C, 61.77; H, 6.01; N, 8.64. Found: C, 61.68; H, 6.12; N, 8.61. UV/vis (1.71×10^{-6} M, CH_2Cl_2): λ_{max}/nm (log ϵ) 406 (5.07), 520 (4.21), 551 (4.16). IR (Nujol, cm^{-1}): "oxidation state marker" band 1018. ^{1}H NMR (300 MHz, CD_2Cl_2): H_{meso} 10.0 (4H, s), CH_2 (eq) 4.07 (16H, q, J = 7.65 Hz), CH_3 (eq) 1.99 (24H, t, J = 7.64 Hz); H_o(ax) 6.48 (4H, d, J = 8.01 Hz), H_m(ax) 4.63 (4H, d, J = 8.25 Hz), CH_3(ax) 2.29 (6H, s). FAB mass spectrum: m/z 972 [M]$^+$, 803 [M − NTs]$^+$, 648 [M − NTs − Ts]$^+$, 634 [M − NTs − NTs]$^+$.

Reactions of [Ru^{VI}(Por)(NTs)$_2$] (2) with Alkenes and Alkanes. General Procedures. All the stoichiometric reactions were carried out under an argon atmosphere by employing standard Schlenk techniques. In a typical run, to a solution of substrate (1−2 mmol) in dichloromethane (2 mL) containing pyrazole (2% w/w) in a 10-mL Schlenk tube was added [Ru^{VI}(Por)(NTs)$_2$] **(2)** (0.05 mmol). The mixture was stirred for 3 h. After removal of the solvent in vacuo, a mixture of *n*-pentane and diethyl ether (5:1 v/v) was added, resulting in formation of a reddish-purple precipitate. The precipitate, which was characterized to be [Ru^{IV}(Por)(NHTs)(pz)] (pz = pyrazolate anion) **(3)** (see below), was collected by filtration and washed with *n*-pentane (yield: ca. 75%). An aliquot of the filtrate, containing organic products, was taken out and mixed with 1-bromo-4-chlorobenzene as internal standard and then analyzed by GC. In the cases where authentic samples of aziridine or amine products were unavailable, the solvent of the filtrate was removed in vacuo, and the residue was purified by chromatography and then analyzed by ^{1}H NMR. The organic products, identified by comparison of their spectral data with those reported in the literature if available[3d] or otherwise independently characterized by ^{1}H NMR and high-resolution mass spectroscopy along with elemental analyses (see Supporting Information), were quantified with the addition of 1,1-diphenylethene as an internal standard. The *cis*-:*trans*-aziridine ratio in the aziridination of *cis*-β-deuteriostyrene was determined from the integration ratio of the appropriate proton resonance: δ = 2.90 and 2.45 ppm for *cis*- and *trans*-β-deuteriostyrene aziridine, respectively.

Characterization of [Ru^{IV}(Por)(NHTs)(pz)] (3). [Ru^{IV}(TPP)(NHTs)(pz)] (3a): Anal. Calcd for $C_{54}H_{39}N_7O_2RuS$: C, 68.20; H, 4.13; N, 10.31. Found: C, 68.40; H, 3.92; N, 10.40. UV/vis (1.56×10^{-6} M, CH_2Cl_2): λ_{max}/nm (log ϵ) 412 (5.07), 530 (3.96), 562 (br) (3.65). IR (Nujol, cm^{-1}): "oxidation state marker" band 1012. ^{1}H NMR (300 MHz, CD_2Cl_2): H_β −17.3 (8H, s), H_o(eq), H_m(eq), H_p(eq) 7.3, 6.9 (20H); NHTs: H_m(ax) 11.8 (2H), H_o(ax) 5.0, CH_3(ax) 8.9 (3H); the NH resonance was not located; pz: H_m(ax′), $H_{m'}$(ax′) −27.5 (1H), −29.4 (1H); the H_o(ax′) resonance was not located. FAB mass spectrum: m/z 951 [M]$^+$, 883 [M − pz]$^+$, 781 [M − NHTs]$^+$, 713 [M − NHTs − pz]$^+$.

[Ru^{IV}(OEP)(NHTs)(pz)] (3b): Anal. Calcd for $C_{46}H_{55}N_7O_2RuS\cdot C_5H_{12}$: C, 64.94; H, 7.16; N, 10.39. Found: C, 64.85; H, 7.20; N, 10.33. UV/vis (1.97×10^{-6} M, CH_2Cl_2): λ_{max}/nm (log ϵ) 343 (4.19), 396 (4.86), 509 (br) (3.80). IR (Nujol, cm^{-1}): "oxidation state marker" band 1020. ^{1}H NMR (500 MHz, CD_2Cl_2): H_{meso} 10.3 (4H), H_a(eq) 15.5 (8H), H_b(eq) 11.4 (8H), CH_3(eq) 1.3 (24H); NHTs: H_m(ax) 10.5 (2H), H_o(ax) 5.6 (2H), CH_3(ax) 7.9 (3H); the NH resonance was not located; pz: H_m(ax′), $H_{m'}$(ax′) −24.3 (1H), −28.4 (1H); the H_o(ax′) resonance was not located. FAB mass spectrum: m/z 871 [M]$^+$, 803 [M − pz]$^+$, 701 [M − NHTs]$^+$, 634 [M − NHTs − pz]$^+$.

Kinetic Studies on the Reaction of [Ru^{VI}(TPP)(NTs)$_2$] (2a) with Alkenes. Kinetic measurements were performed on a Hewlett-Packard 8452A Diode Array spectrophotometer interfaced with an IBM-compatible PC and equipped with a Lauda RM6 circulating water bath by using standard 1.0-cm quartz cuvettes. The temperature of solutions during kinetic experiments was maintained to within ±0.2 °C.

The rates of imido group transfer from **2a** to alkenes were measured by monitoring the decrease of absorbance of **2a** at 536 nm under the condition that the concentration of alkenes was at least 100-fold in excess of the ruthenium complex. Pseudo-first-order rate constants (k_{obs}) were determined by nonlinear least-squares fits of ($A_f - A_t$) to time (t) according to the following equation:

$$(A_f - A_t) = (A_f - A_i)\exp(-k_{obs}t)$$

where A_f and A_i are the final and initial absorbance, respectively, and A_t is the absorbance measured at time t. Kinetic data over 4 half-lives ($t_{1/2}$) were used for the least-squares fitting. Second-order rate constants, k_2, were obtained from the linear fit of the k_{obs} values to the concentration of alkenes.

Activation enthalpy ($\Delta H^{\neq}$) and entropy ($\Delta S^{\neq}$) were obtained from the slope and the intercept, respectively, of the ln(k_2/T) vs (1/T) plot on the basis of the Eyring equation,

$$\ln(k_2/T) = \ln(R/Nh) + \Delta S^{\neq}/R - \Delta H^{\neq}/RT$$

where N is the Avogadro's number, R is the universal gas constant, h is Planck's constant, and T is the temperature in Kelvin (K). The Eyring plots were fit by unweighted linear least-squares methods by using the software package Origin (Microcal Software, Inc.). Errors in the derived activation parameters are the errors of the straight-line fit.

X-ray Crystal Determination of 3b·C$_5$H$_{12}$. Crystals of **3b** were obtained by a slow diffusion of *n*-pentane into a solution of **3b** in chloroform. A purple crystal having dimensions of 0.30 × 0.20 × 0.15 mm mounted on a glass fiber was used for data collection at 301 K on a Rigaku AFC7R diffractometer with graphite monochromatized Mo Kα radiation (λ = 0.71073 Å) using ω−2θ scans with a ω-scan angle (0.73 + 0.35 tan θ)° at a scan speed of 4.0 deg min^{-1} (up to 6 scans for reflection with $I < 15\,\sigma(I)$). Unit cell dimensions were determined based on 25 reflections in the 2θ range of 20.35−25.7°. Intensity data (in the range of $2\theta_{max}$ = 50°; h 0 to 11; k 0 to 21; l −33 to 33; 3 standard reflections measured after every 300 reflections showed decay of 6.45%) were corrected for decay and for Lorentz and polarization effects, and empirical absorption corrections based on the Ψ-scan of five strong reflections (minimum and maximum transmission factors: 0.913 and 1.000, respectively). The space group was determined uniquely based on systematic absences and the structure was solved by Patterson methods and expanded by Fourier methods (PATTY[24]) and refined by full-matrix least-squares using the software package TeXsan[25] on a Silicon Graphics Indy computer. One crystallographic asymmetric unit consists of one formula unit. In the least-squares refinement, 57 non-H atoms of the complex molecule were refined

(24) *PATTY*: Beurskens, P. T.; Admiraal, G.; Beurskens, G.; Bosman, W. P.; Garcia-Granda, S.; Gould, R. O.; Smits, J. M. M.; Smykalla, C. *The DIRDIF program system, Technical Report of the Crystallography Laboratory*; University of Nijmegen: The Netherlands, 1992.

(25) *TeXsan*: *Crystal Structure Analysis Package*; Molecular Structure Corporation: The Woodlands, Texas, 1985 & 1992.

Scheme 2

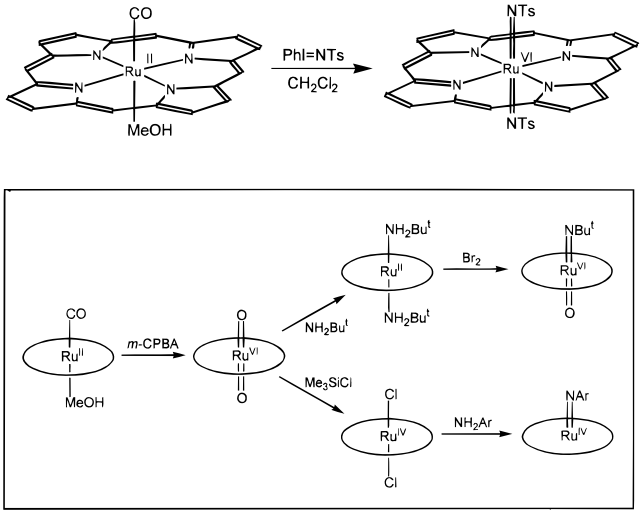

anisotropically, but the 5 C atoms of the *n*-pentane solvent molecule were refined isotropically. The 66 H atoms at calculated positions with thermal parameters equal to 1.3 times that of the attached C atoms were not refined. The final difference Fourier map was featureless, with maximum positive and negative peaks of 1.00 and 0.40 e Å, respectively.

Other Physical Measurements. ^{1}H NMR spectra were recorded on a Bruker DPX 300 or DRX 500 FT NMR spectrometer (300 or 500 MHz, respectively), and chemical shifts (δ, ppm) were reported relative to tetramethylsilane (TMS). Ultraviolet and visible spectra were run on a Perkin-Elmer Lambda 19 spectrophotometer. Infrared spectra were recorded on a Bio-Rad FT-IR spectrometer (Nujol mulls). GC analyses were performed on a HP 5890 Series II system equipped with a HP 5890A flame ionization detector and a HP 3395 integrator. Elemental analyses were performed by Butterworth Laboratories Ltd. (Teddington, Middlesex, U.K.). Fast Atom Bombardment (FAB) mass spectra were recorded on a Finnigan MAT 95 mass spectrometer using 3-nitrobenzyl alcohol as matrix. Electrospray mass spectra were measured on a Finnigan LCQ quadruple ion trap mass spectrometer. Magnetic susceptibility was determined by the Evans method.[26]

Results and Discussion

Bis(tosylimido)ruthenium(VI) Porphyrins [Ru^{VI}(Por)-(NTs)$_2$] (2). i. Synthesis. Treatment of [Ru^{II}(Por)(CO)(MeOH)] (**1**) with slightly excess PhI═NTs in dichloromethane readily afforded the bis(tosylimido)ruthenium(VI) complexes **2** (Scheme 2). The reaction is rather analogous to the oxidation of **1** with excess *m*-CPBA (*m*-chloroperoxybenzoic acid) to give the dioxoruthenium(VI) complexes [Ru^{VI}(Por)O_2].[27] By employing a series of *sterically unencumbered meso*-tetraarylporphyrinato and octaethylporphyrinato ligands, complexes **2a**−**e** were isolated in about 65% yields, demonstrating a good generality of this synthetic route. Very recently, we were informed that Groves and co-workers had prepared, through similar reaction, a bis(tosylimido)ruthenium(VI) complex with the TMP macrocycle, a typical *sterically encumbered* porphyrinato ligand.[19] In contrast to the "one-pot" synthesis of **2**, the previously reported alkyl-[28] and arylimido[29] ruthenium porphyrins were both prepared by a three-step method (Scheme 2), which, however, has been found to be applicable to the *meso*-tetraarylporphyrinato ligands only, and has not led to the isolation of bis(alkyl- or arylimido)ruthenium(VI) porphyrins.

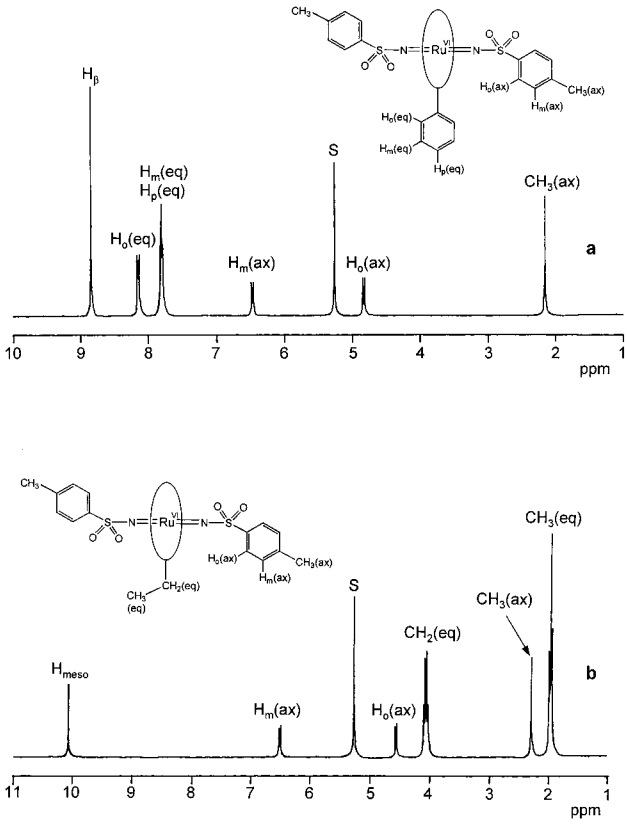

Figure 1. ^{1}H NMR spectra (300 MHz) in CD_2Cl_2 of (a) [Ru^{VI}(TPP)-(NTs)$_2$] (**2a**) and (b) [Ru^{VI}(OEP)(NTs)$_2$] (**2e**).

ii. Characterization. As usual for d^2 ruthenium species, all the complexes **2a**−**e** are diamagnetic, which is revealed by their ^{1}H NMR spectra showing sharp peaks at normal fields. Two typical spectra of **2a** and **2e** are given in Figures 1a and 1b, respectively. The H_β chemical shifts of **2a**−**d** (8.81−8.88 ppm) are close to those observed for oxo(imido)ruthenium(VI) (ca. 8.9 ppm)[28] and dioxoruthenium(VI) (ca. 9.1 ppm)[27e] complexes with the same tetraarylporphyrinato ligands. The H_{meso} chemical shift of **2e** (10.0 ppm) is also comparable to that of its dioxo analogue (10.58 ppm).[27d] The ortho and meta protons of the axial tosyl groups of **2a**−**e** appear as doublets at ca. 4.8 and 6.5 ppm, respectively, which are at considerably higher fields than those of free PhI═NTs, probably due to the porphyrin ring current effect. In all cases the integration ratios are consistent with the bis(tosylimido) formulation of complexes **2**. Furthermore, the whole spectrum of each of **2a**−**d** is extremely similar to that of [Os^{VI}(Por)(NTs)$_2$][30] with the same porphyrinato ligand (the structure of [Os^{VI}(TPP)(NTs)$_2$] has been determined by X-ray crystallographic study[30]).

The para substituents on the *meso*-phenyl groups have little influence on the chemical shifts of the H_β, H_o(eq), and the axial tosyl protons among the imido complexes **2a**−**d**. However, the H_m(eq) chemical shifts are relatively sensitive to such para substituents; for example, the H_m(eq) signal of the complex with chloro substituents (**2c:** 7.73 ppm) is considerably downfield from the corresponding signals of the complexes with electron-donating methyl (**2b:** 7.58 ppm) or methoxy (**2d:** 7.34 ppm) substituents.

(26) Evans, D. F. *J. Chem. Soc.* **1959**, 2003.

(27) (a) Groves, J. T.; Quinn, R. *Inorg. Chem.* **1984**, *23*, 3844. (b) Groves, J. T.; Quinn, R. *J. Am. Chem. Soc.* **1985**, *107*, 5790. (c) Groves, J. T.; Ahn, K.-H. *Inorg. Chem.* **1987**, *26*, 3831. (d) Leung, W.-H.; Che, C.-M. *J. Am. Chem. Soc.* **1989**, *111*, 8812. (e) Ho, C.; Leung, W.-H.; Che, C.-M. *J. Chem. Soc., Dalton Trans.* **1991**, 2933.

(28) Huang, J.-S.; Che, C.-M.; Poon, C.-K. *J. Chem. Soc., Chem. Commun.* **1992**, 161.

(29) Leung, W.-H.; Hun, T. S. M.; Hou, H.-W.; Wong, K.-Y. *J. Chem. Soc., Dalton Trans.* **1997**, 237.

(30) Au, S.-M.; Fung, W.-H.; Huang, J.-S.; Cheung, K.-K.; Che, C.-M. *Inorg. Chem.* **1998**, *37*, 6564.

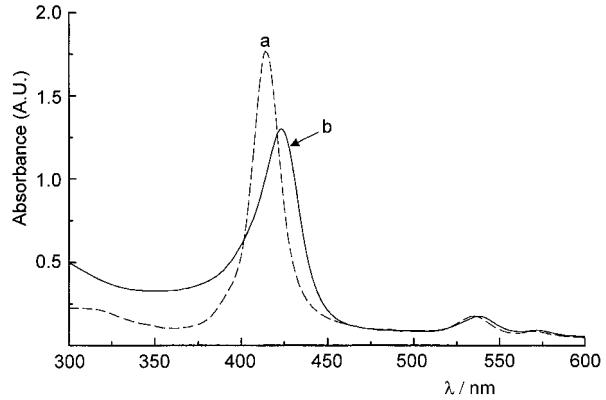

Figure 2. UV−visible spectra in dichloromethane of (a) [Ru^{II}(TPP)(CO)(MeOH)] (9.3×10^{-6} M) and (b) after its complete conversion to [Ru^{VI}(TPP)$(NTs)_2$] (**2a**).

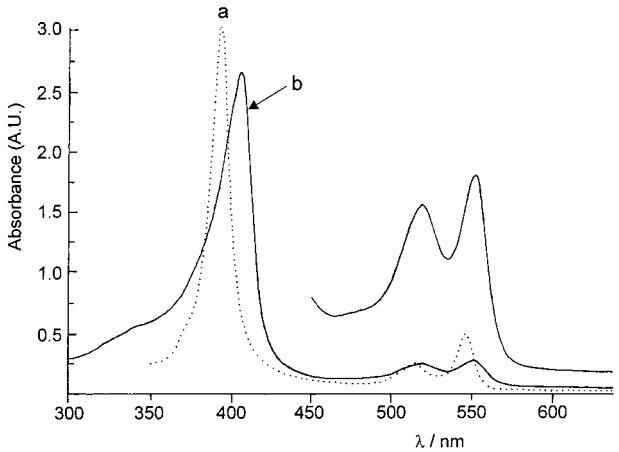

Figure 3. UV−visible spectra in dichloromethane of (a) [Ru^{II}(OEP)(CO)(MeOH)] and (b) [Ru^{VI}(OEP)$(NTs)_2$] (**2e**).

UV/vis measurements reveal that conversion of [Ru^{II}(Por)(CO)(MeOH)] (**1**) to [Ru^{VI}(Por)$(NTs)_2$] (**2**) causes a red shift of the Soret band, as is evident from Figures 2 and 3. This is similar to the conversion from **1** to the dioxo complexes [Ru^{VI}(Por)O_2].[27] However, while the latter conversion appreciably blue shifts the β band, an obvious red shift of this band occurs in the case of the former conversion. On the other hand, the spectra of **2** are considerably different from their osmium analogues, [Os^{VI}(Por)$(NTs)_2$].[30] This is not surprising, since there is also a large difference between the spectra of [Ru^{VI}(Por)O_2] and [Os^{VI}(Por)O_2].[31]

The IR spectra of **2** each exhibit an intense band in the range of 909−920 cm^{-1}, which might correspond to the ruthenium−imido stretching vibrations. These frequencies are lower than those of the osmium−imido bands (950−972 cm^{-1}) found for [Os^{VI}(Por)$(NTs)_2$].[30] The "oxidation state marker" bands for **2a**−**d** appear in the range of 1016−1019 cm^{-1}, similar to those of other ruthenium(VI) porphyrins.[28] The substituents (H, Me, Cl, or MeO) on the *meso*-phenyl rings again have only minor effects on the position of the "oxidation state marker" band.

The FAB^+ mass spectra of **2a**−**e** show the cluster peak attributable to the parent ion, albeit in a weak intensity. Surprisingly, the most prominent peak in each of the spectra corresponds to the fragment $[Ru(Por)N]^+$, identified on the basis of the excellent matching of the observed and simulated isotope distributions, apparently due to the loss of a tosylimido group and the cleavage of the N−Ts bond in the remaining imido group. Even by employing electrospray mass spectrometry, which utilizes a considerably softer ion source, such fragmentation was still significant, although its extent was greatly reduced. Figure 4 shows the positive-ion electrospray mass spectrum of **2e** as an example. As is obvious from this figure, the most intense peak at *m*/*z* 972 corresponds to the parent ion of **2e**. The peak of the fragment $[Ru(OEP)N]^+$ at *m*/*z* 648 becomes weaker but still intense. There are also a few weak peaks in Figure 4, one of which, with *m*/*z* 804, might be ascribed to the monoimido species $\{[Ru(OEP)(NTs)] + H\}^+$ or the amido species $[Ru(OEP)(NHTs)]^+$. The facile formation of nitridoruthenium porphyrins $[Ru(Por)N]^+$ in the gas phase should be very interesting. This suggests a considerable thermal stability of such species, although their isolation has not been realized so far.

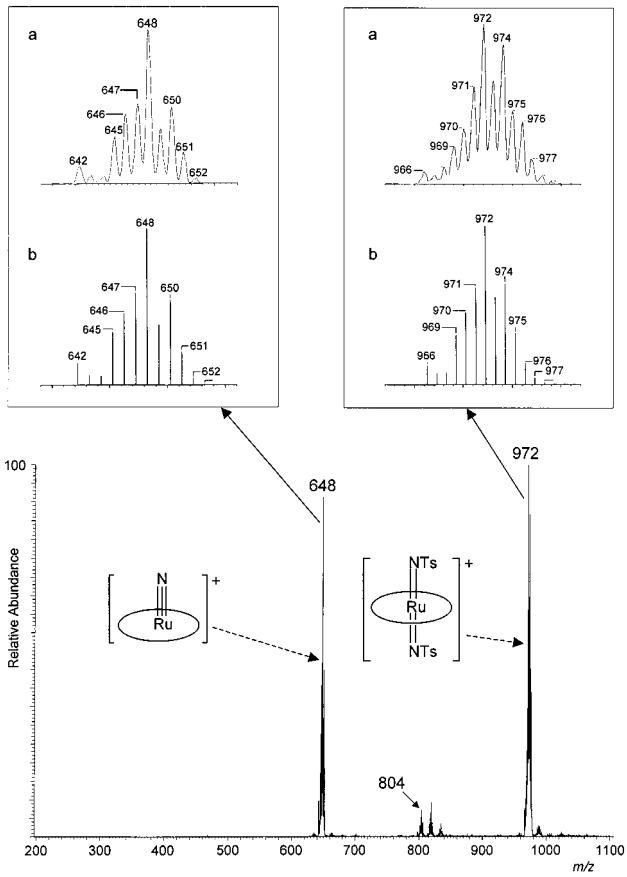

Figure 4. Positive-ion electrospray mass spectrum of [Ru^{VI}(OEP)$(NTs)_2$] (**2e**) in dichloromethane. In the insets are shown (a) the observed and (b) theoretical isotope patterns of the parent ion and the fragment $[Ru(OEP)N]^+$.

iii. Stability and Reactivity. The bis(tosylimido) complexes **2a**−**e** are stable for a few days at ca. −15 °C in the solid state. In highly purified dichloromethane solutions under an inert atmosphere, they could exist for several hours without detectable decomposition. However, upon prolonged standing, **2** became unstable in the solution and gradually degraded into some unknown products. Therefore, we are unable to obtain, despite extensive attempts, diffraction-quality single crystals for **2**. Notably, all these complexes exhibit remarkable stability toward moisture. For example, addition of two drops of water to a solution of **2a** in CD_2Cl_2 in an NMR tube caused no change in the proton resonances of **2a** within a period of ca. 5 h.

All the complexes **2** react rapidly with PPh_3 in dichloromethane at ambient conditions. However, conversion of **2** to mono(tosylimido)ruthenium(IV) porphyrins, [Ru^{IV}(Por)(NTs)],

(31) Che, C.-M.; Cheung, W.-C.; Lai, T.-F. *Inorg. Chem.* **1988**, *27*, 2801.

by treatment with an equimolar amount of PPh_3 seems difficult. In situ ^1H NMR measurements revealed that reaction of **2a** with 1 equiv of PPh_3 afforded a mixture of several products within 5 min, and at least two such products are paramagnetic ruthenium porphyrins (H_β: ca. −16 and −24 ppm, respectively). Attempts to isolate and characterize both species were unsuccessful. Complexes **2** are also reactive toward alkenes and alkanes in dichloromethane. But again, such reactions are rather complicated, as indicated by the *absence* of clean isosbestic points when monitored by UV/vis spectrophotometry, giving rise to intractable ruthenium porphyrin products. In contrast, *in the presence of pyrazole* (2% w/w), the elusive transient ruthenium(IV) species could be effectively trapped by pyrazole to form tosylamido complexes, [Ru^{IV}(Por)(NHTs)(pz)] (**3**), which were isolated in about 75% yields. Especially, under these conditions, the conversions from **2a** to **3a** by almost all the alkenes and alkanes used in this work appear to be smooth, without accumulation of any long-lived intermediates (see the section on kinetic studies).

Charactrization of [Ru^{IV}(Por)(NHTs)(pz)] (3). i. Spectroscopy. It has been reported that ruthenium(IV) porphyrins can be either paramagnetic[27c,d,29,32a,b] or diamagnetic,[32c−e] depending on the nature of the axial ligands. While the bis(diphenylamido)-ruthenium(IV) porphyrin, [Ru^{IV}(3,4,5-MeO-TPP)(NPh_2)$_2$] (3,4,5-MeO-TPP = *meso*-tetrakis(3,4,5-trimethoxyphenyl)porphyrinato dianion), is found to be diamagnetic,[32e] both the tosylamido complexes **3** are paramagnetic. Magnetic susceptibility measurements for **3** by the Evans method gave μ_{eff} of ca. 3.2 μ_B at 300 K, consistent with two unpaired electrons in the ground state of the complexes.

The ^1H NMR spectra of **3a** and **3b** measured at 293 K feature paramagnetically shifted signals, as shown in Figures 5a and 5b, respectively. On the basis of integration ratio and by comparison of Figure 5a with Figure 5b, almost all the signals could be reasonably assigned. In the case of **3a** with the TPP macrocycle, the H_β proton resonances appear as a very broad peak at −17.3 ppm, which is dramatically different from that (8.82 ppm) of the diamagnetic species **2a**. In contrast, the proton resonances of the phenyl groups, H_o(eq), H_m(eq), and H_p(eq), on the porphyrin ring shift upfield by about 1 ppm from those of **2a**. Surprisingly, although the axial ligands in **3a** are not identical, there is no appreciable splitting of the H_o(eq) or H_m(eq) signals. Perhaps the magnetic nonequivalence of H_o(eq) or H_m(eq) protons caused by the unsymmetrical axial ligation is rather small and is not readily observable in this case. Interestingly, the behavior of the OEP macrocycle in **3b** toward the paramagnetic ruthenium(IV) center is very different from that of TPP described above. First, the H_{meso} proton resonances are located as a broad singlet at 10.3 ppm, only very slightly downfield from that of H_{meso} of **2e** (10.0 ppm).[33] Second, the resonances of the methylene protons on the porphyrin ring, which become diastereotropic due to the lack of mirror symmetry in the ring plane,[34] clearly split into two broad singlets at 15.5 and 11.4 ppm in a 1:1 ratio, although the separation of 4.1 ppm between these two singlets is considerably smaller than that (>10 ppm) found for the paramagnetic [Ru^{II}(OEP)]$_2$.[34]

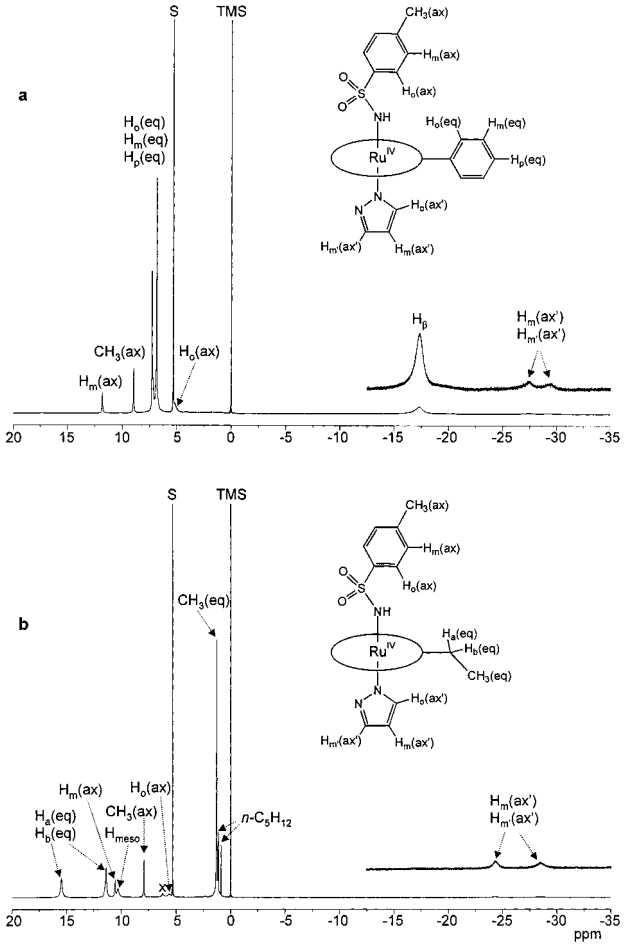

Figure 5. ^1H NMR spectra (500 Hz) in CD_2Cl_2 at 293 K of (a) [Ru^{IV}-(TPP)(NHTs)(pz)] (**3a**) and (b) [Ru^{IV}(OEP)(NHTs)(pz)] (**3b**).

Despite the above differences between TPP and OEP macrocycles, the proton resonances of the axial ligands in **3a** and **3b** are fairly similar in both their chemical shifts and line shapes. For both complexes, the H_m(ax), CH_3(ax), and H_o(ax) signals of the tosylamido axial ligands appear at ca. 11, 8, and 5 ppm, respectively, whereas the H_m(ax′) and $H_{m'}$(ax′) signals of pyrazolate axial ligands appear at ca. −26 and −28 ppm. The resonances of H_o(ax′) of pyrazolate axial ligands were not located, which might be too broad to be observed owing to their short distances to the paramagnetic center.

The "oxidation state marker" band in the IR spectrum of **3a** is located at 1012 cm^{-1}, identical with that observed for [Ru^{IV}-(3,4,5-MeO-TPP)(NPh_2)$_2$] (1012 cm^{-1}).[32e] As compared with the UV/vis spectrum of **2a**, **3a** exhibits appreciably blue-shifted Soret and β bands. Such is also the case for **3b** vs **2e**. The Soret band of **3a** at 412 nm is similar to those reported for the arylimidoruthenium(IV) porphyrins.[29] The formulation of **3** as a ruthenium porphyrin bearing both tosylamido and pyrazolato axial ligands is also inferred by their FAB mass spectra, which exhibit the cluster peak attributable to the desired parent ion, and their elemental analyses. The structure of **3a** has been determined by X-ray crystal analysis and reported in the previous communication.[10]

(32) (a) Ke, M.; Sishta, C.; James, B. R.; Dolphin, D.; Sparapany, J. W.; Ibers, J. A. *Inorg. Chem.* **1991**, *30*, 4766. (b) Cheng, S. Y. S.; Rajapakse, N.; Rettig, S. J.; James, B. R. *J. Chem. Soc., Chem. Commun.* **1994**, 2669. (c) Collman, J. P.; Brothers, P. J.; McElwee-White, L.; Rose, E. *J. Am. Chem. Soc.* **1985**, *107*, 6110. (d) Collman, J. P.; Brothers, P. J.; McElwee-White, L.; Rose, E.; Wright, L. J. *J. Am. Chem. Soc.* **1985**, *107*, 4570. (e) Huang, J.-S.; Che, C.-M.; Li, Z.-Y.; Poon, C.-K. *Inorg. Chem.* **1992**, *31*, 1315.

(33) We noted that the H_{meso} chemical shifts of paramagnetic ruthenium-(IV) porphyrins could in some cases be very similar to those of related diamagnetic complexes. For example, the H_{meso} chemical shifts of the paramagnetic [Ru^{IV}(OEP)X_2] (X = Br, Cl, F) were found to be 3.50, 8.89, and 9.63 ppm, respectively,where the last is very similar to the H_{meso} chemical shift of the diamagnetic [Ru^{IV}(OEP)Ph_2] (9.68 ppm). See: Sishta, C.; Ke, M.; James, B. R.; Dolphin, D. *J. Chem. Soc., Chem. Commun.* **1986**, 787.

(34) Collman, J. P.; Barnes, C. E.; Swepston, P. N.; Ibers, J. A. *J. Am. Chem. Soc.* **1984**, *106*, 3500.

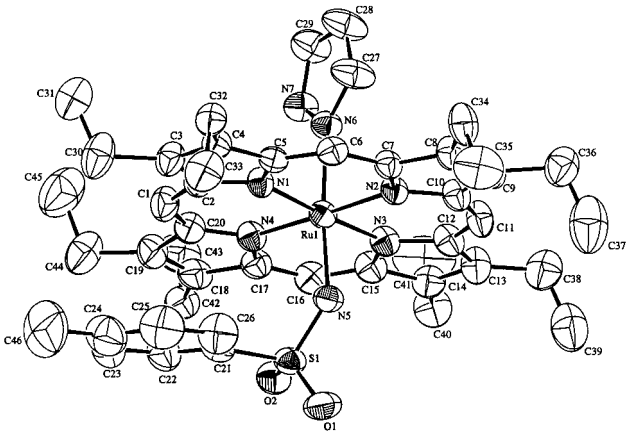

Figure 6. ORTEP drawing of $[Ru^{IV}(OEP)(NHTs)(pz)]$ (**3b**)·C_5H_{12} with the atom-numbering scheme. Hydrogen atoms and the solvent molecule are omitted for clarity. Thermal ellipsoids are drawn at the 35% probability level.

Table 1. Structure Determination Summary

empirical formula	$C_{46}H_{55}N_7O_2SRu·C_5H_{12}$
formula weight	943.27
cryst syst	monoclinic
space group	$P2_1/c$ (No. 14)
a, Å	9.847(4)
b, Å	17.938(6)
c, Å	28.405(6)
β, deg	96.55(3)
V, Å^3	4984(2)
Z	4
F(000)	1992
T, K	301
density (calcd), g/cm^3	1.257
abs coeff, cm^{-1}	4.01
data collected	$h, k, \pm l$
no. of reflns collected	9664
no. of independent reflns	9100
no. of obsd reflns ($I > 3\sigma(I)$)	4908
no. of params, P	534
R^a	0.054
$R_w{}^b$	0.081
goodness-of-fit	2.64
$(\Delta/\sigma)_{max}$	0.05

^{a} $R = \sum||F_o| - |F_c||/\sum|F_o|$. ^{b} $R_w = [\sum w||F_o| - |F_c||^2/\sum w|F_o|^2]^{1/2}$.

Table 2. Selected Bond Distances (Å) and Angles (deg) for $[Ru^{IV}(OEP)(NHTs)(pz)]$ (**3b**)·C_5H_{12}

Ru1−N1	2.040(5)	Ru1−N2	2.056(5)
Ru1−N3	2.035(6)	Ru1−N4	2.056(5)
Ru1−N5	2.020(6)	Ru1−N6	2.085(6)
N5−S1	1.587(6)	S1−O1	1.451(6)
S1−O2	1.426(5)	S1−C21	1.802(8)
N5−Ru1−N6	173.1(2)	Ru1−N5−S1	135.6(3)
N1−Ru1−N2	90.1(2)	N1−Ru1−N4	89.9(2)
N3−Ru1−N2	90.1(2)	N3−Ru1−N4	89.8(2)
N5−Ru1−N1	92.4(2)	N5−Ru1−N2	84.4(2)
N5−Ru1−N3	91.3(2)	N5−Ru1−N4	97.1(2)
N6−Ru1−N1	88.1(2)	N6−Ru1−N2	88.7(2)
N6−Ru1−N3	88.2(2)	N6−Ru1−N4	89.7(2)

ii. X-ray Crystal Structure of 3b·C_5H_{12}. The ORTEP drawing of **3b**, together with the atom-numbering scheme, is depicted in Figure 6. Crystallographic data for the structure determination and selected bond distances and angles are listed in Tables 1 and 2, respectively. The porphyrin ring is basically planar, whose component atoms have a mean deviation of 0.0277 Å from the least-squares plane. The eight ethyl groups on the porphyrin ring assume an *aaaabbbb* conformation (Figure 7a). The ruthenium(IV) ion is essentially in the porphyrin ring plane, with Ru−N(Por) distances ranging from 2.035(6) to 2.056(5) Å. As is evident from Figure 7b, the S1, N5, Ru1, N2, and N4 atoms are basically coplanar. However, the pyrazolate ring rotates from this plane by ca. 17°. The Ru1−N5 and Ru1−N6 distance of 2.020(6) and 2.085(6) Å, respectively, and the Ru−N5−S1 angle of 135.6(3)° are all similar to the corresponding distances or angle found in **3a**.[10]

Kinetic Studies on the Reactions of $[Ru^{VI}(TPP)(NTs)_2]$ (2a) with Alkenes. The UV/vis spectral changes for the reaction of **2a** with excess styrene in dichloromethane containing pyrazole (2% w/w) are shown in Figure 8, which reveals a decrease in absorbance of the Soret band of **2a** and a concomitant increase in absorbance of a new Soret band at 412 nm. The final spectrum is virtually identical with that of the amido complex **3a**. The appearance of isosbestic points at 446, 518, and 552 nm suggests that the conversion of **2a** to **3a** is a simple kinetic process without accumulation of any long-lived intermediates. A similar phenomenon has also been observed for the reactions of **2a** with all the other alkenes, except *cis*-/*trans*-stilbenes, used in the kinetic studies.

Under similar conditions, the reaction of **2e**, containing OEP macrocycle, with styrene in the presence of pyrazole is somewhat different. The UV/vis spectral changes show isosbestic points at 378, 438, 510, 527, 538, and 565 nm at the early stage but become more complicated as the reaction proceeds to completion. Again, the final spectrum is virtually identical with that of **3b**. It seems that the conversion of **2e** to **3b** involves at least two distinct steps.

The reaction of **2a** with alkenes follows the first-order rate law under the pseudo-first-order conditions: [alkene] (0.2−1.8 M) ≫ [**2a**] (1.6×10^{-5} M). In all cases, k_{obs} is linearly dependent on [alkene], and the slopes of such plots give the second-order rate constants (k_2). The absence of kinetic saturation (even at high concentration of alkenes) indicates that a prior coordination of alkene to **2a**, e.g. via a π-complex, is either absent or unimportant. Values of k_2, so determined, are listed in Table 3. In most cases, the k_2 values are larger than those reported for the epoxidation of the same alkenes by $[Ru^{VI}(TPP)O_2]$.[27e] It should be noted that, *in the absence of alkenes*, ***2a*** *exhibited no appreciable reaction with pyrazole under the same conditions on the time scale of the kinetic studies*.

Examination of Table 3 reveals that both electronic and steric effects are operating in the imido group transfer reactions between **2a** and alkenes. For example, the k_2 values observed for methylstyrenes follow the order *p*-methylstyrene > styrene > *cis*-β-methylstyrene > *trans*-β-methylstyrene > α-methylstyrene. This order cannot be rationalized on the basis of the nucleophilicity of the alkenes alone. Among all these methylstyrenes, *p*-methylstyrene should have the least steric hindrance because of the remote location of the methyl group from the reaction site. Therefore, the larger rate of the imido group transfer to this substrate than to styrene almost entirely results from an electronic effect. This suggests that electron-donating substituents on the alkenes favor such transfer processes, and the attack by **2a** toward alkenes is electrophilic. In the cases of other methylstyrenes, the methyl group is directly or closely linked to the reaction site, which renders them even more nucleophilic, but also much more sterically demanding, than *p*-methylstyrene. Here, the steric effect should be responsible for the smaller k_2 values observed for these substrates.

Studies of the effect of temperature on the k_{obs} values for the imido group transfer reactions between **2a** and two representative alkenes afforded linear Eyring plots over a temperature

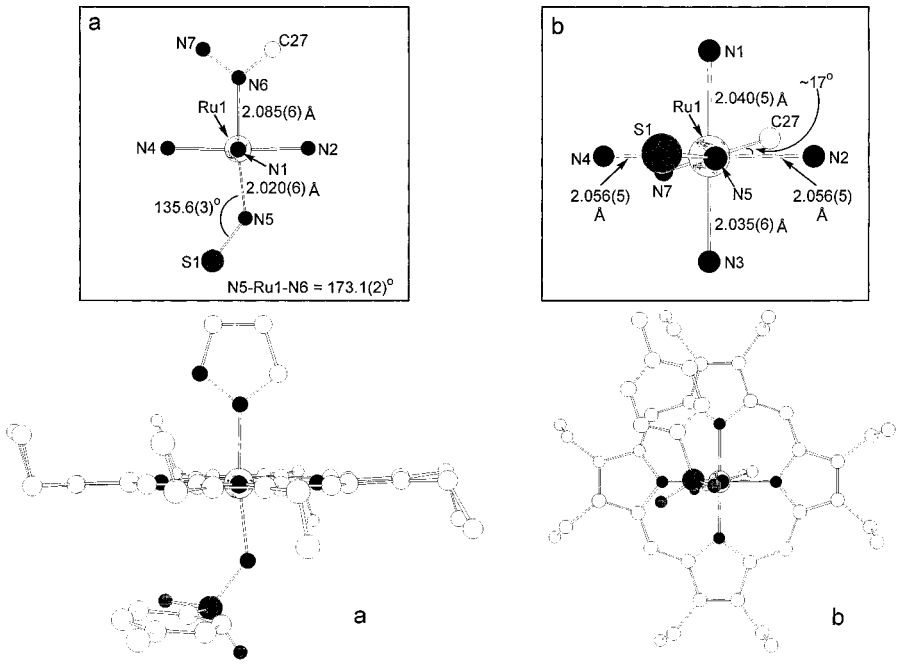

Figure 7. Ball and stick drawing of **3b** showing (a) the *aaaabbbb* conformation of the eight ethyl groups on the porphyrin ring and (b) the orientations of tosylamido and pyrazolate axial ligands with respect to the porphyrinato ligand. The insets a and b depict the core structures in (a) and (b), respectively.

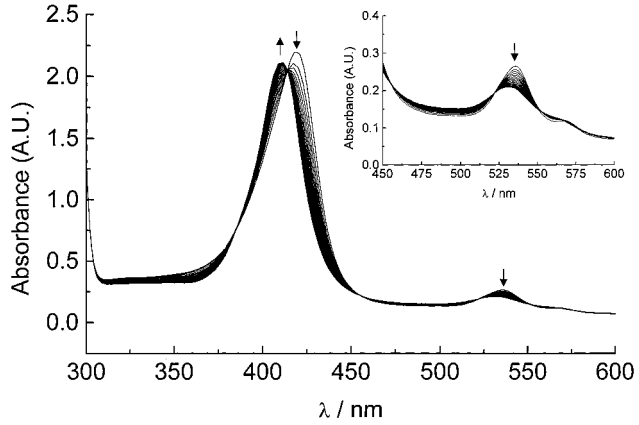

Figure 8. UV−visible spectral changes during the reaction of [Ru^{VI}(TPP)$(NTs)_2$] (**2a**) (1.6×10^{-5} M) with styrene (0.19 M) in dichloromethane containing pyrazole (2% w/w) at 298 K. Scans were taken at 30-s intervals.

range of 288−318 K. The activation enthalpies $\Delta H^{\neq}$ and entropies $\Delta S^{\neq}$ for *cis*-cyclooctene and styrene by **2a** are listed in Table 4. The large negative $\Delta S^{\neq}$ values in both cases suggest an association of reactants in the transition states.

Stoichiometric Reactions of [Ru^{VI}(Por)$(NTs)_2$] (2) with Alkenes. i. Product Analysis. The stoichiometric reactions were carried out by using higher concentrations of **2** and alkene than those used for the kinetic studies to increase the concentrations of the products. The product yields, based on the amount of **2** used, for different alkenes are summarized in Table 5. In the cases of aziridination of styrene by **2a**−**d**, the product yields range from 75 to 80%, which are rather insensitive to the nature of para substituents on the *meso*-phenyl groups of the porphyrinato ligand. In contrast, reaction of **2e** with styrene afforded *N*-(*p*-tolylsulfonyl)-2-phenylaziridine in 85% yield. The improved yield in this case may be ascribed to the relatively open reaction site in the complex bearing OEP ligand.

It is noteworthy that the reactions of **2** with alkenes also afforded tosylamide ($TsNH_2$), and in most cases, a mass balance

Table 3. Second-Order Rate Constants (k_2) for the Imido Group Transfer Reactions between Alkenes and [Ru^{VI}(TPP)$(NTs)_2$] (**2a**) in Dichloromethane Containing Pyrazole (2% w/w) at 298 K

entry	alkene	$10^3 k_2$/dm^3 mol^{-1} s^{-1}
1	*cis*-cyclooctene	2.80 ± 0.07
2	norbornene	5.1 ± 0.1
3	2,3-dimethyl-2-butene	17.0 ± 0.4
4	styrene	9.0 ± 0.1
5	*p*-methoxystyrene	90 ± 4
6	*p*-methylstyrene	16.0 ± 0.8
7	*p*-fluorostyrene	11 ± 1
8	*p*-chlorostyrene	8.8 ± 0.1
9	*p*-acetoxystyrene	5.4 ± 0.1
10	*p*-trifluoromethylstyrene	3.2 ± 0.2
11	*p*-cyanostyrene	1.60 ± 0.06
12	α-methylstyrene	4.8 ± 0.1
13	*trans*-β-methylstyrene	5.2 ± 0.2
14	*cis*-β-methylstyrene	6.8 ± 0.1
15	α-d_1-styrene	9.3 ± 0.2
16	β-d_2-styrene	10.6 ± 0.2

Table 4. Activation Parameters for the Imido Group Transfer Reactions between Alkenes and [Ru^{VI}(TPP)$(NTs)_2$] (**2a**)

alkene	$\Delta H^{\neq}$/kcal mol^{-1}	$\Delta S^{\neq}$/eu
cis-cyclooctene	10.0 ± 0.3	−(36.5 ± 1.7)
styrene	5.1 ± 0.2	−(50.7 ± 3.2)
cumene	10.2 ± 0.2	−(37.5 ± 1.6)
ethylbenzene	8.9 ± 0.2	−(39.8 ± 2.0)
cyclohexene	7.2 ± 0.3	−(43.9 ± 2.3)

of aziridine and $TsNH_2$ is close to 100%, a phenomenon similar to that observed previously for the imido group transfer reactions catalyzed by iron or manganese porphyrins.[2] Moreover, we found that the *N*-tosylaziridine:$TsNH_2$ ratio can be markedly increased in anhydrous conditions. Unlike the imido group transfer of PhI═NTs to aromatic alkenes catalyzed by iron porphyrins,[2] only trace amounts of epoxide and benzaldehyde were detected except for the aziridination of *trans*- and *cis*-stilbene. The reaction of **2a** with *trans*-stilbene gave *trans*-*N*-(*p*-tolylsulfonyl)-2,3-diphenylaziridine in low yield. No *cis*-aziridine was detected. The low product yields from the

Table 5. Stoichiometric Imido Group Transfer Reactions between Alkenes and $[Ru^{VI}(TPP)(NTs)_2]$ (**2a**) or $[Ru^{VI}(OEP)(NTs)_2]$ (**2e**) in Dichloromethane Containing Pyrazole (2% w/w)

substrate	product		yield(%)[a] 2a	2e
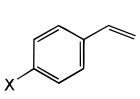	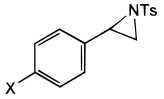	X = H	75	85
		X = MeO	82	
		= Me	78	
		= F	72	
		= Cl	71	
		= CH_3COO	71	
		= CF_3	69	
		= CN	67	
	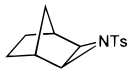		68	71
	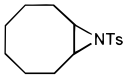		66	70
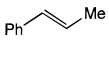	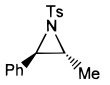		72	76
			(*trans*-)[b]	
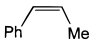	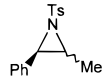		75	
			(*trans*:*cis* = 66:34)[b]	
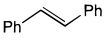	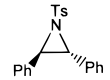		10	17
			(*trans*:*cis* > 97:3)[b]	
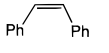	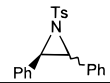		22	
			(*trans*:*cis* = 86:14)[b]	

[a] Isolated yield of aziridine based on **2a** and **2e** used. [b] Ratios of trans:cis *N*-tosylaziridine were determined by 300-MHz ^{1}H NMR spectroscopy.

aziridination of *trans*-and *cis*-stilbene by **2a** probably reflect a lower reactivity of **2a** toward both of the alkenes. However, of significance are notable amounts of *trans*-stilbene oxide found in the reaction of **2a** with either *trans*- or *cis*-stilbene.

ii. Reaction Stereospecificity. The stereospecificity in metal-mediated aziridination of *cis*-alkenes provides important information on the mechanism of such a process. Mansuy and co-workers reported that aziridination of *cis*-stilbene by PhI═NTs catalyzed by iron or manganese porphyrins exclusively afforded the corresponding *trans*-aziridine, and the nonstereospecificity of these reactions is consistent with a stepwise mechanism, i.e., the formation of an acyclic intermediate that is sufficiently long-lived to undergo the cis−trans isomerization through rotation about the related C−C single bond.[2b] In contrast, the stereospecific $CuClO_4$-catalyzed aziridination by PhI═NTs of unfunctionalized alkyl-substituted alkenes such as *cis*-4-octene reported by Evans and co-workers argued for a concerted mechanism.[3d]

We have found that aziridinations of *cis*-alkenes by **2a** are generally nonstereospecific, with the formation of a mixture of *cis*- and *trans*-aziridines in ratios of 14:86, 25:75, and 50:50 (based on ^{1}H NMR analyses) for aziridination of *cis*-stilbene, *cis*-*β*-methylstyrene, and *cis*-*β*-deuteriostyrene, respectively. These ratios were reproducible by repeating the reactions for at least three times. The purity of the *cis*-alkenes (>99%) had been checked by GC prior to use, indicating the absence of *trans*-alkenes. At the end of the reactions, *trans*-alkenes were again not detected by either GC or ^{1}H NMR. It is noteworthy that such a cis−trans isomerization unlikely results from an isomerization of aziridine catalyzed by the Ru(IV) product **3a**. For example, after stirring a mixture of pure *cis*-N-(*p*-tolylsulfonyl)-2-methyl-3-phenylaziridine and **3a** in dichloromethane for 3 h under identical conditions, the starting *cis*-aziridine remained unchanged and the corresponding *trans*-aziridine was not detected.

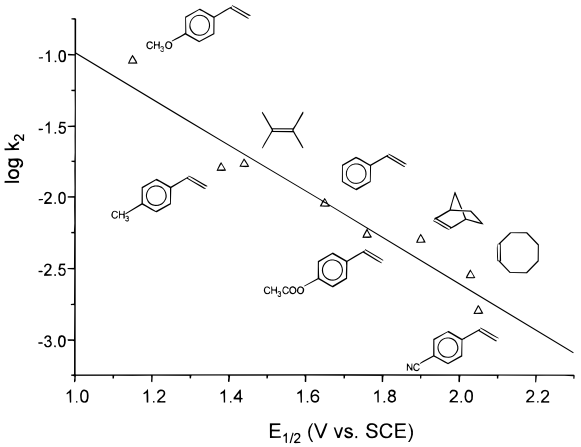

Figure 9. Plot of the log of the second-order rate constant (k_2) for the reaction of $[Ru^{VI}(TPP)(NTs)_2]$ (**2a**) with a series of eight alkenes vs the 1e oxidation potential ($E_{1/2}$) of the alkenes.

Evidently, the aziridination of *cis*-alkenes by **2a** results in only a *partial loss* of the alkene stereochemistry, in contrast to the iron and manganese porphyrin-catalyzed aziridination of *cis*-stilbene by PhI═NTs, in which a *complete loss* of alkene stereochemistry was observed.[2] The imido group transfer reactions between **2a** and *cis*-alkenes may involve both concerted and stepwise pathways. However, the clean second-order kinetics observed for the reactions between **2a** and styrene or *cis*-*β*-methylstyrene is incompatible with the operation of multiple reaction pathways. Inasmuch as the loss of alkene stereochemistry is hard to reconcile with a concerted mechanism, a stepwise pathway analogous to that proposed by Mansuy and co-workers[2b] should be operative for the aziridination reactions by **2a**. The cis:trans ratio 14:86 for the aziridination of *cis*-stilbene is low, perhaps due to a severe steric interaction between the *cis*-phenyl groups in the proposed acyclic intermedieate, which will greatly favor the C−C bond rotation to form the *trans*-aziridine.

The Nature of the Rate-Determining Step. i. The Correlation between k_2 and $E_{1/2}$. To get further information on the nature of the transition state at the rate-determining step, we examined the correlation between the second-order rate constant (k_2) of the reaction of **2a** with an alkene and the 1e oxidation potential ($E_{1/2}$) of the alkene for all the alkenes in Table 3 whose $E_{1/2}$ values are available.[17e] The log k_2 vs $E_{1/2}$ plot is shown in Figure 9, which exhibits a good linearity with k_2 and $E_{1/2}$ ranging from 1.6×10^{-3} to 9.0×10^{-2} M^{-1} s^{-1} and 1.15−2.05 V, respectively. It has been established that, for a reaction proceeding via an initial single electron transfer and showing a linear free-energy correlation between log k_2 and $E_{1/2}$, the slope of the log k_2 vs $E_{1/2}$ plot should be (i) zero if the diffusion together of the reactants is rate limiting, (ii) -16.6 V^{-1} if the 1e transfer is extremely endothermic, and (iii) in the range of 0 to -16.6 V^{-1} in other cases.[35] The slope in Figure 9 was determined to be -1.7 V^{-1}, corresponding to a slope of $\alpha = 0.1$ in the conventional Bronsted plot (log k_2 vs log K_{eq}). Obviously, there is little charge transfer from the alkenes to **2a** in the transition state. Therefore, a mechanism involving rate-limiting 1e tranfer to form an alkene-derived π-cation radical (**III**) can be dismissed. For comparison, the slope of the log k_2

(35) (a) Rehm, D.; Weller, A. *Isr. J. Chem.* **1970**, *8*, 259. (b) Andrieux, C. P.; Blocman, C.; Dumas-Bouchiat, J.-M.; Saveant, J.-M. *J. Am. Chem. Soc.* **1979**, *101*, 3431.

Scheme 3

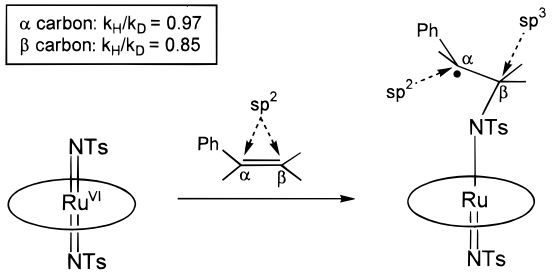

vs $E_{1/2}$ plot was reported to be -2.99 V^{-1} for the epoxidation of alkenes by [$(Br_8TPP)Cr^V(O)(ClO_4)$] involving the rate-determining formation of a charge-transfer complex[17e] and -0.89 V^{-1} for the epoxidation of alkenes by [$(Cl_8TPP)Mn^{IV}$-(O)] where neutral carbon-radical was formed.[17h]

The involvement of the azametallacyclobutane intermediate (**II**), an analogue of metallaoxetane, in the rate-determining step might be plausible. However, the following observations seem to argue against the intermediacy of such species. Since the UV/vis spectral changes for the reactions of **2a** with all the alkenes in Figure 9 exhibit clean isosbestic points, there should be no accumulation of any long-lived intermediate during these reactions. On the other hand, molecular modeling studies by Bruice and co-workers revealed that, in the case of alkene epoxidation by hypervalent metal-oxo porphyrins, the formation of metallaoxetanes would result in severe steric interactions.[17g] It is unlikely that replacing the oxo group by the bulkier tosylimido group will ease the congested spatial environment. Moreover, the formation of intermediate **II** hinges on a seven-coordinate ruthenium center, which is almost unprecedented in ruthenium porphyrin chemistry.

ii. Isotope Effect. The measurement of secondary kinetic deuterium isotope effect can provide information about the hybridization changes occurring at an isotopically substituted carbon atom as a set of reactants pass from their ground states to the transition states.[36] In the case of alkene aziridination, two sp^2 carbons become more sp^3-like in the aziridine product. If either intermediate **I** or **II** is involved in the reaction, then a simultaneous rehybridization of both α and β carbon atoms of alkenes, such as styrene, from sp^2 to sp^3 is required. However, the isotope effect data obtained from the reactions of **2a** with styrene and deuteriostyrenes show a clear distinction between the α and β carbons in the transition state: only the β-carbon atom changes its hybridization from sp^2 to sp^3 ($k_H/k_D = 0.85$), while the α-carbon atom remains essentially sp^2 hybridized ($k_H/k_D = 0.97$). The k_H/k_D value of 0.85 observed for the β-carbon falls in the range of k_H/k_D values (0.82−0.95) found for the same carbon atom from the competitive epoxidation of styrene and *cis*-β-deuteriostyrene catalyzed by [Mn(salen)Cl].[17m] This implies that in the transition state there is a substantial C_β−N but negligible C_α−N bond formation (Scheme 3), which serves as an additional argument against both the concerted mechanism involving intermediate **I** and the stepwise pathway that involves intermediate **II**.

iii. Substitution Effect. The effect of para substituents on the rates of the imido group transfer of **2a** to styrene and its derivatives has been investigated. The log's of the relative rates (k_R) obtained for several para-substituted styrenes (*p*-Y-C_6H_4-$CHCH_2$, Y = OMe, Me, F, H, Cl, CF_3, and CN) are summarized in Table 6. It is evident from this table that substituted styrenes with electron-donating substituents are more reactive than styrene, whereas electron-withdrawing substituents retard the imido group transfer process. Fitting (by the least-squares method) the log k_R data in Table 6 to σ^+ scale results in good linearity ($R = 0.98$) (Figure 10) with a ρ^+ value of -1.1,[10] indicating a minor influence of the electronic effect of para substituents on the k_2 values. This again argues against the involvement of the alkene-derived cation radical **III**. The involvement of the carbocation intermediate **IV** is also unlikely, since the rate-limiting formation of carbocations in the electrophilic addition to the C=C bond has ρ^+ values as negative as -3.5 (hydration)[37a] and -4.1 (bromination).[37b] However, such a small variation of the rate constants with para substituents observed in this work might be expected for the rate-limiting formation of the carboradical intermediate **V**.

Table 6. Variation of log k_R with σ_p^+, σ_{mb}, and $\sigma_{JJ}^\bullet$ Scales for the Aziridination of Para-Substituted Styrenes by [Ru^{VI}(TPP)$(NTs)_2$] (**2a**)

p-X	log *k* (exptl)	σ_p^+	σ_{mb}	$\sigma_{JJ}^\bullet$	log k_R(calcd)[a]
OMe	1	−0.778	−0.77	0.233	0.928
Me	0.25	−0.311	−0.29	0.15	0.382
F	0.087	−0.073	−0.24	−0.02	0.241
H	0	0	0	0	0
Cl	−0.00976	0.114	0.11	0.22	−0.00044
CF_3	−0.449	0.53	0.49	−0.01	−0.519
CN	−0.75	0.66	0.86	0.42	−0.682

[a] log k_R(calcd) = $-1.05\sigma_{mb} + 0.522\sigma_{JJ}^\bullet$.

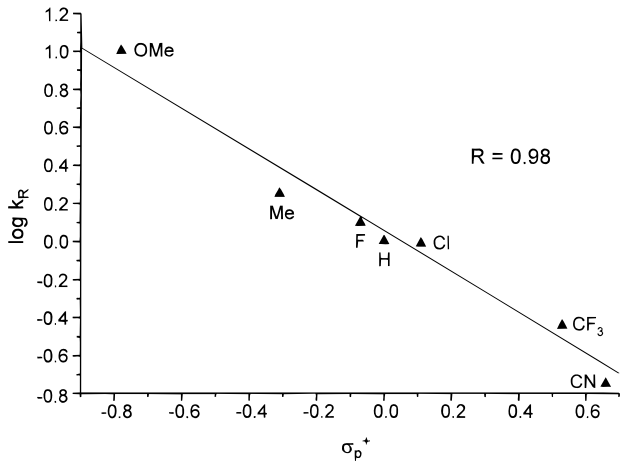

Figure 10. Linear-free-energy correlation of log k_R vs σ^+ for the reactions of [Ru^{VI}(TPP)$(NTs)_2$] (**2a**) with a series of *para*-subsituted styrenes at 298 K.

According to the above studies on isotope effect, for the aziridination of para-substituted styrenes, the carboradical intermediates **V** if really involved should contain a para-substituted benzyl radical moiety, in which a significant spin-delocalization might exist.[38] Indeed, a careful examination of the log k_R vs σ^+ plot in Figure 10 reveals some sizable deviations of the log k_R values (for the substituents OMe, Me, and CN) from the single-parameter regression. After considering the spin-delocalization effect by employing the $\sigma_{JJ}^\bullet$ scale recently developed by Jiang and co-workers, the log k_R vs (σ_{mb}, $\sigma_{JJ}^\bullet$) plot[38] gives rise to an appreciably better linearity ($R = 0.99$), as shown in Figure 11. It is likely that the spin-delocalization effect does exist. Multiple linear regression for the dual-

(36) Collin, C. J.; Bowman, N. S. *Isotope Effects in Chemical Reactions*; Van Nostrand Reinhold: New York, NY, 1970.

(37) (a) Schubert, W. M.; Keefe, J. R. *J. Am. Chem. Soc.* **1972**, *94*, 559. (b) Yates, K.; McDonald, R. S.; Shapiro, S. A. *J. Org. Chem.* **1973**, *38*, 2460.

(38) Jiang, X.-K. *Acc. Chem. Res.* **1997**, *30*, 283.

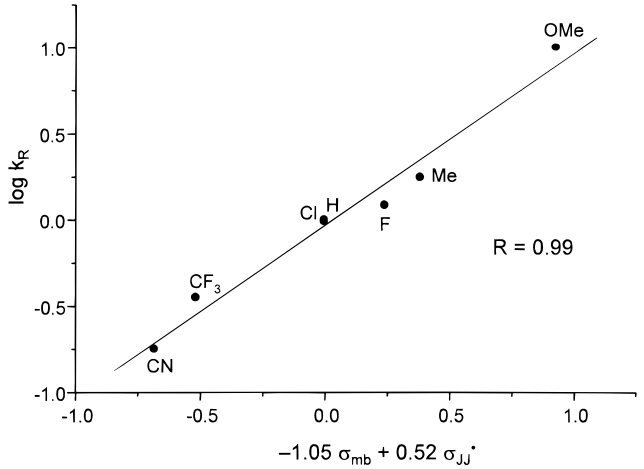

Figure 11. Linear-free-energy correlation of log k_R vs (σ_{mb}, $\sigma_{JJ}^{\bullet}$) for the reactions of [Ru^{VI}(TPP)$(NTs)_2$] (**2a**) with a series of para-subsituted styrenes at 298 K.

Scheme 4

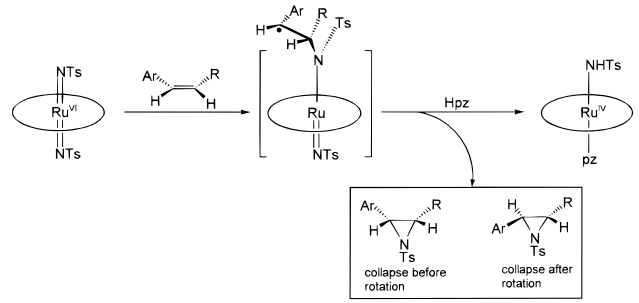

parameter equation[38]

$$\log k_R = \rho_{mb}\sigma_{mb} + \rho_{JJ}^{\bullet}\sigma_{JJ}^{\bullet}$$

gives the values of ρ_{mb} and $\rho_{JJ}^{\bullet}$ of −1.05 and +0.52, respectively. The positive $\rho_{JJ}^{\bullet}$ value reveals that all the para substituents delocalize the spin in the transition state. On the other hand, the negative ρ_{mb} suggests that the attacks toward the alkenes are all electrophilic. In addition, the $|\rho_{mb}/\rho_{JJ}^{\bullet}|$ ratio of 2.02, which is considerably larger than unity, indicates that the polar effect is dominant in the imido group transfer reactions.[38]

We, therefore, postulate that the alkene aziridination by **2a** should occur via the rate-limiting formation of the carboradical intermediate **V** (Scheme 4). This type of intermediates could undergo C−C bond rotation prior to the ring closure to produce aziridines. Analogous carboradical intermediates have also been proposed in the aziridination of alkenes by PhI═NTs catalyzed by iron porphyrins albeit without kinetic evidence,[2b] and also in the epoxidation of alkenes by d^2 dioxoruthenium(VI) porphyrins.[27e] Since the imido complex **2a** exhibits no appreciable reaction with water at room temperature within several hours, as described above, the tosylamide byproduct in the reactions between **2a** and alkenes should not result from a prehydrolysis of **2a** but may arise from the reaction of the carboradical species with protic reagents.

Tosylamidation of C−H Bonds. Imido group transfer reactions of complexes **2** have been observed not only with alkenes but also with alkanes, leading to formation of tosylamides as a result of insertion of the tosylimido group into the C−H bonds. In the case of a saturated alkane, tosylamidation is selectively directed toward the tertiary C−H bonds. For example, the reactions of **2a,e** with adamantane afforded *N*-(1-adamantyl)-tosylamide in 52 and 60% yield, respectively. In contrast, cyclohexane, which lacks a tertiary C−H bond, was tosylamidated by **2a,e** to give cyclohexylamide in poor yields (about 10%), comparable to its tosylamidation by PhI═NTs catalyzed by iron and manganese porphyrins.[11] Interestingly, the phenyl substitution dramatically improves the reactivity of C−H bonds of an alkane toward complexes **2**. Despite the lack of a tertiary C−H bond, ethylbenzene was tosylamidated by **2a,e** to give α-(*N*-tosylamino)ethylbenzene in yields as high as 80%. Listed in Table 7 are the product yields for the tosylamidation of a variety of hydrocarbons by **2a,e** under the same conditions.

Table 7. Stoichiometric Tosylamidation of Hydrocarbons by [Ru^{VI}(TPP)$(NTs)_2$] (**2a**) and [Ru^{VI}(OEP)$(NTs)_2$] (**2e**) in Dichloromethane Containing Pyrazole (2% w/w)

substrate	product	yield(%)[a,b] 2a	2e
	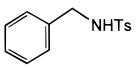	9	11
	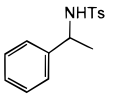	78	80
	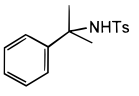	71	77
		84	88
	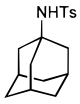	52	60
		~ 10	

[a] Yield based on **2a** and **2e** used. [b] The sum of the yields of the tosylamidation product and $TsNH_2$ is about 100%.

The UV/vis spectral change during the reaction of **2a** with ethylbenzene in dichloromethane containing pyrazole (2% w/w) is depicted in Figure 12. The final product was identified to be **3a** as aforementioned. Plots of k_{obs} vs [hydrocarbon] are shown in Figure 13. The second-order rate constants (k_2) are summarized in Table 8. The activation enthalpy $\Delta H^{\neq}$ and entropy $\Delta S^{\neq}$, determined over the temperature range of 285−305 K, for the tosylamidation of cumene, ethylbenzene, and cyclohexene are listed in Table 4. The large negative $\Delta S^{\neq}$ values suggest an association of reactants in the transition states.

The Nature of the Rate-Determining Step. i. Selectivity Ratio and Steric Effect. It can be seen from Table 8 that tosylamidation of the tertiary C−H bond in cumene is considerably slower than that of the secondary C−H bond in ethylbenzene. On the basis of the ratio of the k_2 values of cumene and ethylbenzene (Table 8) and by taking the statistical factor into account, a selectivity ratio, *k*[tertiary(C−H)]/*k*[secondary(C−H)], of 0.84 was obtained, which is *less than* unity and substantially smaller than that of 2.9 obtained for the oxidation of the C−H bonds in the same substrates by [Ru^{VI}(TPP)O_2].[27e] Such an unusually small selectivity ratio might result from a steric effect. Since the tosylimido group is much larger than the oxo group, there might be a significant steric hindrance in

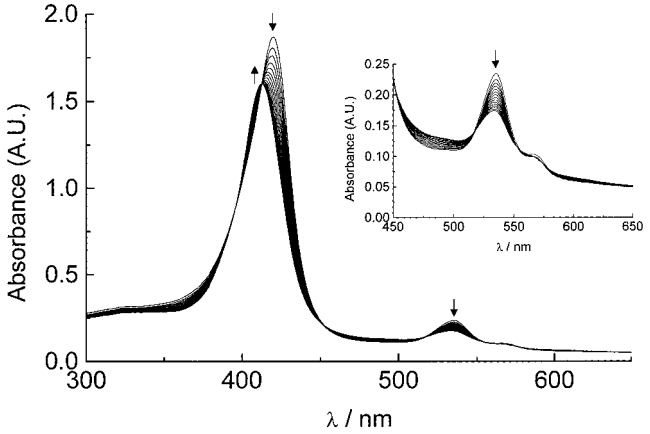

Figure 12. UV−visible spectral changes observed during the reaction of $[Ru^{VI}(TPP)(NTs)_2]$ (**2a**) (1.3×10^{-5} M) with ethylbenzene (0.19 M) in dichloromethane containing pyrazole (2% w/w) at 298 K. Scans were taken at 60-s intervals.

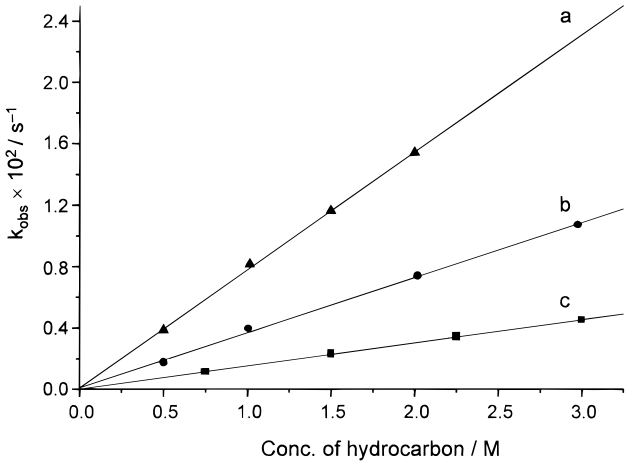

Figure 13. Plots of k_{obs} vs [hydrocarbon] for the tosylamidation of (a) cyclohexene, (b) ethylbenzene, and (c) cumene by $[Ru^{VI}(TPP)(NTs)_2]$ (**2a**).

Table 8. Summary of Second-Order Rate Constants for the Tosylamidation of Hydrocarbons by $[Ru^{VI}(TPP)(NTs)_2]$ (**2a**)

entry	hydrocarbon	$10^3 k_2$/dm^3 mol^{-1} s^{-1}
1	cumene	1.5 ± 0.1
2	ethylbenzene	3.60 ± 0.07
3	ethylbenzene-d_{10}	0.330± 0.008
4	cyclohexene	7.7 ± 0.3
5	cyclohexene-d_{10}	1.30 ± 0.04
6	*p*-methoxyethylbenzene	16.5 ± 0.3
7	*p*-methylethylbenzene	6.8 ± 0.1
8	*p*-chloroethylbenzene	5.0 ± 0.1
9	*p*-fluoroethylbenzene	4.3 ± 0.1

the transition state of the tosylamidation of cumene by **2a** due to the presence of a methyl group at the reaction site.

ii. Isotope Effect. Reactions involving C−H bond cleavage in the transition states usually exhibit a large primary kinetic isotope effect.[39] Indeed, for the tosylamidation of ethylbenzene by **2a**, a k_H/k_D of 11 was obtained, which is identical or very close to the corresponding values found for the oxidation of C−H bonds by *cis*-$[Ru^{VI}(Tet\text{-}Me_6)(O)_2]^{2+}$ (Tet-Me$_6$ = *N*,*N*,*N*′,*N*′-tetramethyl-3,6-diazaoctane-1,8-diamine) (k_H/k_D = 11)[39c] and *trans*-$[Ru^{VI}(pytn)(O)_2]^{2+}$ (pytn = *N*,*N*′-dimethyl-*N*,*N*′-bis(2-pyridylmethyl)propylenediamine) (k_H/k_D = 12).[39b] The isotope effect for the tosylamidation of cyclohexene by **2a** was somewhat smaller, with a k_H/k_D ratio of 6.1. All these k_H/k_D values are typical for H-atom abstraction reactions to form carboradical intermediates.[39]

Table 9. Variation of log k_R with TE for the Tosylamidation of Para-Substituted Ethylbenzenes by $[Ru^{VI}(TPP)(NTs)_2]$ (**2a**)

p-X	TE	log k_R
OMe	1.08	0.662
Me	0.42	0.273
Cl	0.23	0.145
F	0.16	0.078
H	0.00	0.0

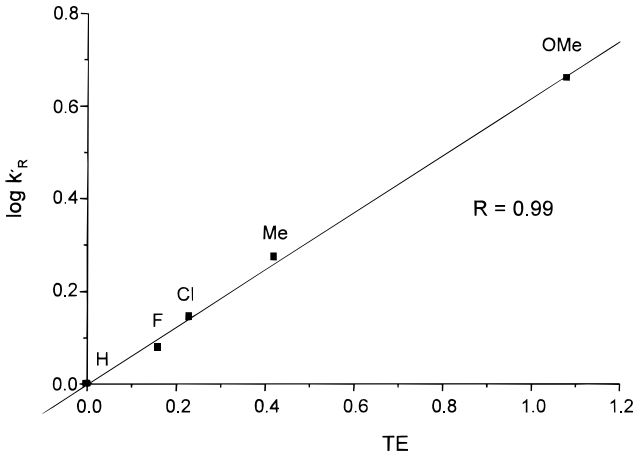

Figure 14. Linear-free-energy correlation of log k_R vs TE for the reactions of $[Ru^{VI}(TPP)(NTs)_2]$ (**2a**) with a series of para-substituted ethylbenzenes at 298 K.

iii. Substitution Effect. Studies of the effect of para substituents on the rate of tosylamidation of ethylbenzene by **2a** reveal that both electron-donating and -withdrawing substituents promote the reaction. However, the overall influence of the para substituents on the relative rates is minor, as shown in Table 9, which is incompatible with the intermediacy of either alkene-derived cation radical or carbocation intermediates in the rate-determining step.

It is likely that the rate-determining step of the tosylamidation by **2a** involves a carboradical intermediate. To obtain further evidence for this, we examined the correlation between the relative reactivity data (log k_R) and TE, i.e., the substitution effect on the C−H bond dissociation energy.[40] The TE (total effect) parameters have been calculated by Wu and co-workers by the density functional method for a series of para-substituted toluene, which are the differences between the substituent effects on the stability of radical (RE) and ground state (GE).[40] The TE values used in this work are listed in Table 9. The log k_R vs TE plot depicted in Figure 14 exhibits very good linearity (R = 0.99) with a $\rho_{TE}^{\bullet}$ value of +0.62 (the slope). This provides added support for the rate-limiting formation of a benzylic radical intermediate in the tosylamidation of ethylbenzene.

On the basis of the above results, we propose a mechanism for the tosylamidation reactions by complex **2a** as depicted in Scheme 5. Abstraction of a hydrogen atom by the ruthenium imido complex should occur on the periphery of the complex, since the imido moiety is bound to the coordinately and electronically saturated ruthenium center. Subsequently, the radicals produced are efficiently scavenged by the ruthenium

(39) (a) Che, C.-M.; Leung, W.-H.; Li, C.-K.; Poon, C.-K. *J. Chem. Soc., Dalton Trans.* **1991**, 379. (b) Che, C.-M.; Tang, W.-T.; Wong, K.-Y.; Li, C.-K. *J. Chem. Soc., Dalton Trans.* **1991**, 3277. (c) Cheng, W.-C.; Yu, W.-Y.; Li, C.-K.; Che, C.-M. *J. Org. Chem.* **1995**, *60*, 6840.

(40) Wu, Y.-D.; Wong, C.-L.; Chan, K. W.-K.; Ji, G.-Z.; Jiang, X.-K. *J. Org. Chem.* **1996**, *61*, 746.

Scheme 5

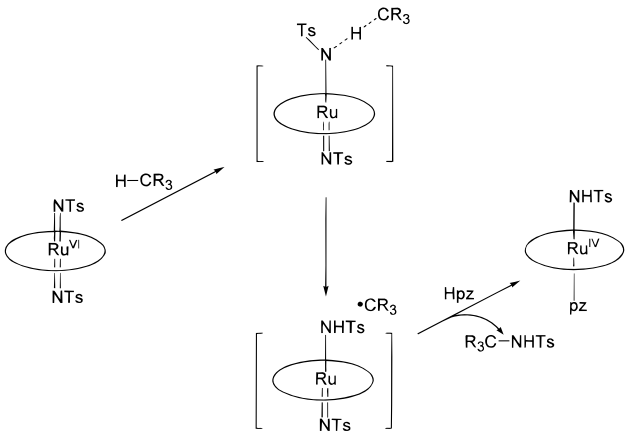

porphyrin. The large deuterium isotope effect supports the symmetrical transition state for the hydrogen atom abstraction.[39]

Conclusion

(1) Treatment of [Ru^{II}(Por)(CO)(MeOH)] (**1**) with PhI═NTs in dichloromethane provides a general, convenient route to the preparation of bis(tosylimido)ruthenium(VI) porphyrins [Ru^{VI}(Por)$(NTs)_2$] (**2**). Complexes **2a**−**e** (Por = TPP, TTP, 4-Cl-TPP, 4-MeO-TPP, and OEP, respectively), isolated in 60−74% yields, have been characterized by ^{1}H NMR, UV/vis, IR, FAB, and electrospray mass spectroscopy along with elemental analyses.

(2) The isolated high-valent ruthenium tosylimido complexes **2a**−**e** can undergo imido group transfer reactions with a series of alkenes and alkanes in dichloromethane containing pyrazole. After these reactions, **2a,e** are converted into paramagnetic tosylamidoruthenium(IV) porphyrins [Ru^{IV}(Por)(NHTs)(pz)] (**3**). The structures of complexes **3a,b** (Por = TPP and OEP, respectively) have been determined by X-ray crystallography.

(3) Reactions of **2a** and **2e** with 12 alkenes afford the corresponding *N*-tosylaziridines in 66−85% yields. The aziridination of *cis*-alkenes, such as *cis*-stilbene and *cis*-*β*-methylstyrene, is nonstereospecific with a partial loss of the alkene stereochemistry. Kinetic studies reveal that the reactions between **2a** and 16 alkenes have the second-order rate constants (k_2) ranging from $(1.60 \pm 0.06) \times 10^{-3}$ to $(90 \pm 4) \times 10^{-3}$ dm^3 mol^{-1} s^{-1} at 298 K, which can be rationalized on the basis of electronic and steric effect.

(4) The above aziridination reactions probably proceed via a stepwise mechanism involving the rate-determining formation of a carboradical intermediate according to the following lines of evidence: (i) The slope of the linear plot of log k_2 vs $E_{1/2}$ for eight representative alkenes was found to be -1.7 V^{-1} (corresponding to $\alpha = 0.1$ in the conventional Bronsted plot), a value too small to be accommodated to a mechanism with rate-limiting formation of an alkene-derived π-cation radical. (ii) In the case of para-substituted styrenes, linear correlation between log k_R (k_R = relative rate) and σ^+ gives a ρ^+ value as small as -1.1, which is hard to reconcile with the rate-determining formation of the π-cation radical or a carbocation intermediate. The fact that the para-substitution effect can be best accounted for by considering both polar and spin-delocalization effects suggests the involvement of a carboradical at the rate-determining step. (iii) The secondary deuterium isotope effect k_H/k_D was found to be 0.85 and 0.97 for the *β*- and α-carbon atom of styrene, respectively, implying that there is a substantial C_β−N but negligible C_α−N bond formation in the transition state. This argues against both the concerted mechanism and the stepwise pathway involving an azametallacyclobutane intermediate.

(5) Reactions of **2a** and **2e** with adamantane, cyclohexene, ethylbenzene, and cumene result in tosylamidation of these hydrocarbons, affording the corresponding tosylamides in 52−88% yields. For cyclohexane and toluene, the tosylamidation products were formed in poor yields (ca. 10%). Kinetic studies on the reactions between [Ru^{VI}(TPP)$(NTs)_2$] and nine hydrocarbons give the second-order rate constants (k_2) in the range of $(0.330 \pm 0.008) \times 10^{-3}$ to $(16.5 \pm 0.3) \times 10^{-3}$ dm^3 mol^{-1} s^{-1}.

(6) The above tosylamidation reactions probably proceed via a rate-determining formation of a carboradical intermediate. First, these reactions exhibit a large primary deuterium isotope effect ($k_H/k_D = 11$) for the tosylamidation of ethylbenzene, indicative of a substantial C−H bond cleavage at the rate-limiting step. Second, in the case of para-substituted ethylbenzenes, both electron-donating and -withdrawing substituents promote the reaction; however, the overall influence is minor. Furthermore, there is a very good linear correlation between log k_R and a related carboradical parameter.

Acknowledgment. This work was supported by the Hong Kong University Foundation and the Hong Kong Research Grants Council. We are grateful to Dr. K.-K. Cheung for the X-ray structural determinations of complex **3b**.

Supporting Information Available: UV−visible spectral changes during the reaction of **2e** with styrene in dichloromethane containing pyrazole; plots of k_{obs} vs [alkene] for reactions of **2a** with styrene, norbornene, *cis*-cyclooctene, *p*-methylstyrene, *cis*-*β*-methylstyrene, *trans*-*β*-methylstyrene, and α-methylstyrene; UV−visible spectrum of **3b** in dichloromethane; characterization of some of the organic aziridine and amine products; and tables of final coordinates, bond lengths, bond angles, and anisotropic displacement parameters of **3b**·C_5H_{12} (PDF). This material is available free of charge via the Internet at http://pubs.acs.org.

JA9913481